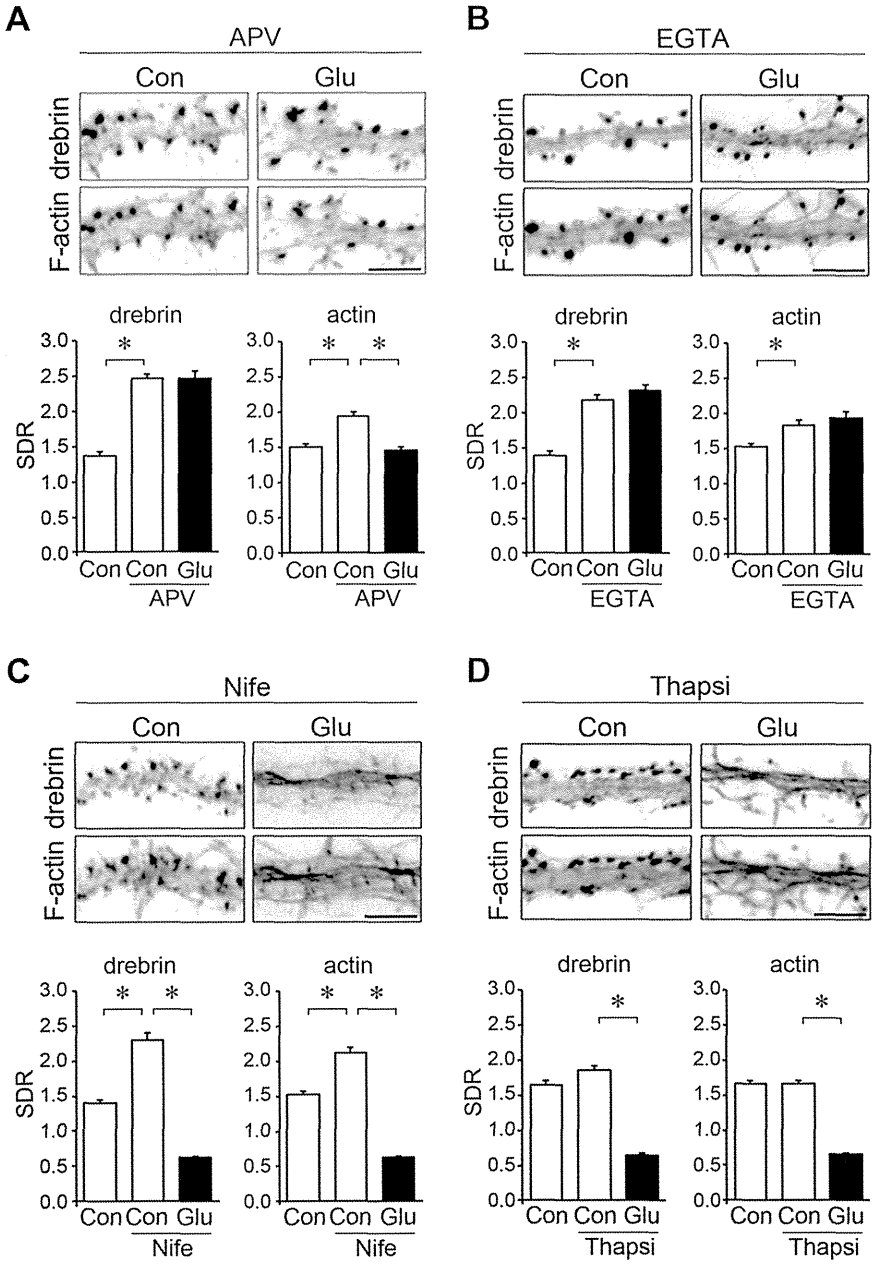

Figure 6. Effects of various inhibitors of Ca^{2+} entry on DA-actin distribution. Neurons (21 DIV) were incubated in normal medium containing 50 μM APV (A), 20 mM EGTA (B), 20 μM nifedipine (C), or 1 μM thapsigargin (D) for 30 min. The neurons were then stimulated with 100 μM glutamate for an additional 10 min. F-actin images indicate that spines kept their structure during the experiment although their shapes were changed. Scale bars, 5 μm. (**A**) APV pretreatment significantly increased both the drebrin and actin SDRs (n = 30 cells; $p<0.01$, Scheffe's test). In the presence of APV, glutamate stimulation significantly decreased the actin SDR (n = 30 cells; $p<0.01$, Student's *t* test) but not the drebrin SDR (n = 30 cells; $p = 0.52$, Student's *t* test). (**B**) EGTA significantly increased the drebrin and actin SDRs (n = 30 cells; $p<0.01$, Scheffe's test), and blocked the glutamate-induced decreases in drebrin and actin SDRs (n = 30 cells; Student's *t* test). (**C**) Nifedipine significantly increased the drebrin and actin SDRs (n = 30; $p<0.01$, Scheffe's test), but did not block the glutamate-induced decrease in drebrin and actin SDRs (n = 30; $p<0.01$, Scheffe's test). (**D**) Thapsigargin neither increased the drebrin and actin SDRs (n = 30; Student's *t* test) nor blocked the glutamate-induced decreases in drebrin and actin SDRs (n = 30; $p<0.01$, Scheffe's test). Error bars represent s.e.m.
doi:10.1371/journal.pone.0085367.g006

light chain kinase (MLCK). When MLCK activity was inhibited with 10 μM ML-7, glutamate stimulation induced the loss of drebrin and F-actin from dendritic spines (photomicrographs in Fig. 8A). Quantitative analysis showed that the ML-7 treatment did not change the drebrin and actin SDR levels compared with control neurons, and did not inhibit the glutamate-induced decreases in the drebrin and actin SDRs (Fig. 8A).

We then inhibited ROCK activity with 1 μM H-1152. In the presence of H-1152, glutamate stimulation induced the loss of drebrin and F-actin from dendritic spines (photomicrographs in Fig. 8B). Quantitative analysis showed that the H-1152 treatment did not change the drebrin and actin SDR levels compared with control neurons, and did not inhibit the glutamate-induced decreases in the drebrin and actin SDRs (Fig. 8B).

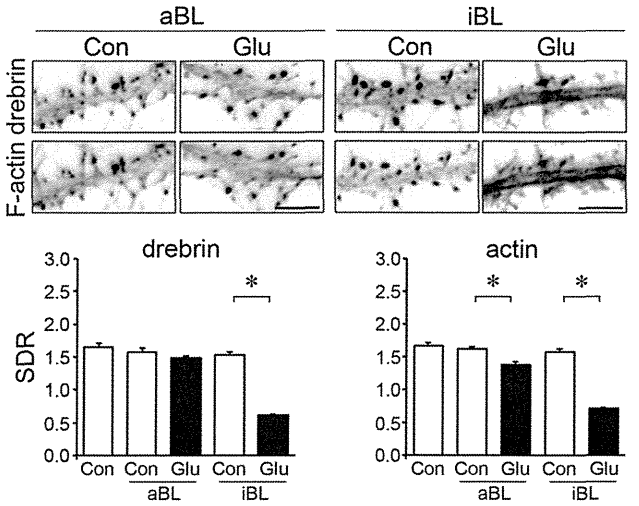

Figure 7. Glutamate-induced DA-actin exodus is blocked by an inhibitor of myosin II ATPase. Neurons (21 DIV) were preincubated with 100 μM aBL for 30 min and then stimulated with 100 μM glutamate for 10 min. F-actin images indicate that spines kept their structure during the experiment although their shapes were changed. Scale bars, 5 μm. The drebrin SDR of aBL-treated neurons was not decreased by glutamate stimulation (n = 30 cells; p = 0.06, Student's *t* test), although that of iBL-treated neurons was decreased (n = 30 cells: p<0.01, Scheffe's test). On the other hand, the actin SDR of aBL-pretreated neurons was slightly, but significantly, decreased by glutamate stimulation (n = 30 cells; p<0.01, Scheffe's test), although the reduction was much smaller than that observed in iBL-pretreated neurons (n = 30 cells; p<0.01, Student's *t* test). Error bars represent s.e.m.
doi:10.1371/journal.pone.0085367.g007

Because MLCK and ROCK phosphorylate MLC [33], the above data suggest that MLC phosphorylation is not involved in the DA-actin exodus.

Discussion

In the present study we demonstrated that (1) chemical long-term potentiation (cLTP) stimulation induces rapid DA-actin exodus and subsequent DA-actin re-entry in dendritic spines, (2) Ca^{2+} influx through NMDA receptors regulates both the exodus and the basal accumulation of DA-actin, and (3) the DA-actin exodus is blocked by a myosin II ATPase inhibitor, but is not blocked by either MLCK or ROCK inhibitors.

These results indicate that Ca^{2+} influx through NMDA receptors induces the DA-actin exodus in LTP induction, and that myosin II mediates the interaction between NMDA receptor activation and DA-actin exodus (Fig. S2). Furthermore, the Ca^{2+} influx seems to activate myosin II ATPase by a rapid actin-linked mechanism instead of slow MLC phosphorylation. Thus the myosin II-mediated DA-actin exodus might be an initial event in LTP induction, triggering actin polymerization and spine enlargement.

SDR analysis of DA-actin migration in and out of dendritic spines

In the present study, using drebrin SDR, we found that APV treatment not only inhibits the DA-actin exodus but also facilitates the accumulation of DA-actin in dendritic spines. In our previous studies, we could not detect any facilitative effect of APV treatment on drebrin accumulation in dendritic spines, because we used drebrin cluster density along dendrites for assessing the dynamic changes in drebrin localization [13,17]. Although this method is sensitive enough to detect the loss of drebrin from

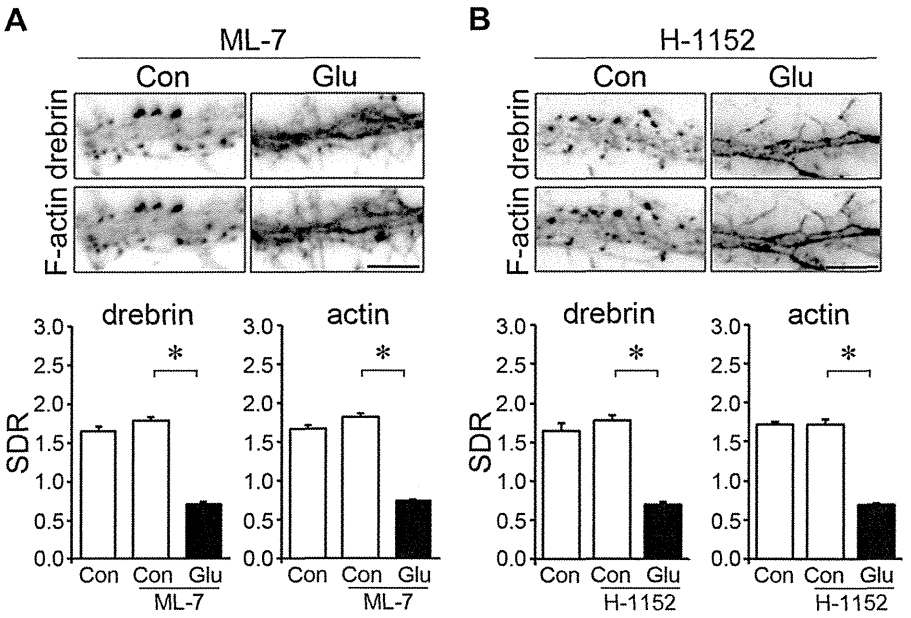

Figure 8. The DA-actin exodus is not blocked by inhibitors of myosin light chain kinase (MLCK) or Rho-associated kinase (ROCK). Neurons (21 DIV) were preincubated with 10 μM of ML-7, an inhibitor of MLCK (A) or 1 μM H-1152, an inhibitor of ROCK (B) for 30 min, and then stimulated with 100 μM glutamate for 10 min. Neither ML-7 (n = 30 cells; drebrin SDR p<0.01, actin SDR p<0.01, Scheffe's test) nor H1152 (n = 30 cells; drebrin SDR p<0.01, actin SDR p<0.01, Scheffe's test) blocked the DA-actin exodus. F-actin images indicate that spines kept their structure during the experiment although their shapes were changed. Scale bars, 5 μm.
doi:10.1371/journal.pone.0085367.g008

dendritic spines, it is not sensitive enough to detect the accumulation of drebrin in dendritic spines.

By comparing the changes in drebrin and actin SDRs we can extrapolate the changes in non-DA-actin, because the total F-actin shown by the actin SDR consists of DA-actin and non-DA-actin. In the present study we found that the glutamate-induced exoduses of DA-actin and non-DA-actin are differentially regulated by each glutamate receptor subtype. Thus measurement of SDR is a useful method to analyze the migration of proteins in and out of dendritic spines.

The DA-actin exodus may trigger the facilitation of F-actin polymerization in dendritic spines

After NMDA receptor activation in LTP induction, facilitation of actin polymerization and spine enlargement are observed [34–35]. However, the underlying mechanisms of these processes have not been elucidated. The present study shows that the total amount of F-actin in dendritic spines transiently decreases shortly after cLTP stimulation, resulting from a DA-actin exodus. Once the total F-actin in dendritic spines reduces by the DA-actin exodus, monomeric actin is likely to immediately refill the vacant space by diffusion [15]. The increase in the amount of monomeric actin is known to facilitate F-actin polymerization [36]. In addition, the treadmilling rate of DA-actin is low [8], suggesting that the high level of DA-actin in dendritic spines makes the average treadmilling rate of total F-actin lower in resting dendritic spines. Because quickly-treadmilling non-DA-actin predominates in dendritic spines after the DA-actin exodus, the average treadmilling rate of total F-actin is increased. Together, it is indicated that the DA-actin exodus increases the monomeric actin content and the treadmilling rate of F-actin in dendritic spines, resulting in the facilitation of F-actin polymerization and spine enlargement (Fig. S2).

Possible molecular mechanism for how Ca^{2+} influx activates myosin II ATPase in dendritic spines

Myosin II ATPase is known to be activated by MLC phosphorylation or by an actin-linked mechanism. The important issue remaining is which molecular mechanism is related to the DA-actin exodus. MLCK and ROCK are two major candidates for the regulator of MLC phosphorylation [33]. The present study reveals that block of neither MLCK nor ROCK inhibits the DA-actin exodus. This finding suggests that MLC phosphorylation is not involved in the DA-actin exodus.

Thus activation of myosin II ATPase by an actin-linked mechanism is likely involved in the DA-actin exodus. In the actin-linked mechanism, myosin II ATPase is activated by the release of the suppressed actomyosin interaction. In mammalian skeletal muscles, when Ca^{2+} binds to the troponin complex, the actomyosin interaction suppressed by tropomyosin is released, and consequently myosin II ATPase is activated. Because drebrin A inhibits the myosin II ATPase activity similar to tropomyosin [20], drebrin A is thought to be the counterpart of tropomyosin in dendritic spines [14]. Therefore it is suggested that drebrin A protects actin filaments from the interaction with myosin II in the resting dendritic spines, resulting in the inhibition of myosin II ATPase. Once NMDA receptors are activated, the Ca^{2+} influx through NMDA receptors may change the location of drebrin A on the actin filaments, releasing the actomyosin interaction suppressed by drebrin A. Consequently myosin II ATPase is activated in dendritic spines. Thus myosin II ATPase activation by an actin-linked mechanism may be an underlying molecular mechanism for the DA-actin exodus.

Furthermore, the present data shows that the DA-actin exodus occurs immediately after cLTP stimulation. The activation of myosin II ATPase by an actin-linked mechanism occurs within 20 ms after stimulation [37]. Thus the myosin-II mediated DA-actin exodus might be an initial event in LTP induction, triggering actin polymerization and spine enlargement.

Role of DA-actin re-entry into dendritic spines

DA-actin re-entry follows the DA-actin exodus. In the present study we found that the LTP-induced DA-actin exodus triggers F-actin polymerization and spine enlargement. The DA-actin re-entry may be related to maintenance of LTP. After the DA-actin re-entry, the dynamic and stable F-actin pools are probably reestablished in the dendritic spines. As a result, polymerization and depolymerization of F-actin is balanced in dendritic spines and the enlarged spine morphology is maintained (Fig. S2). In fact, long lasting increases in F-actin and drebrin content in dendritic spines have been reported when LTP is maintained *in vivo* [38].

What are the underlying mechanisms of DA-actin re-entry? Reduction of the Ca^{2+} influx into dendritic spines might induce the DA-actin re-entry, because the basal accumulation of DA-actin is negatively regulated by Ca^{2+} influx through NMDA receptors and voltage-dependent Ca^{2+} channels in resting spines. Another possible mechanism is a signaling cascade linked to AMPA receptors. LTP stimulation is known to increase the AMPA receptor density in dendritic spines [39]. Because AMPA receptor activity facilitates accumulation of DA-actin in the dendritic spines of immature neurons [17], AMPA receptors might also be involved in the DA-actin re-entry in mature neurons.

Supporting Information

Figure S1 Effects of glutamate stimulation on the density of spines and presynaptic terminals. (**A**) DiI staining of hippocampal neurons. Fixed cultures on coverslips were bathed in PBS and placed on the stage of an inverted phase microscope. Individual cells were stained with 1,1′-dioctadecyl-3,3,3′,3′-tetramethylindocarbocyanine perchlorate (DiI; Molecular Probes, Inc., Eugene, OR). The DiI was dissolved in vegetable oil to saturation, loaded into a glass micropipette (Eppendorf), and applied by pressure ejection onto the multipolar neurons. The coverslips were then placed at room temperature in small petri dishes containing PBS. After 12–24 h, which allowed for sufficient transport of the dye, cells were examined by fluorescence microscopy. The spine morphology of boxed areas in upper panels are shown at higher magnification in middle panels. Note that the spines kept their structures during the experiment. Scale bars, 10 μm. Left panel in the bottom shows the density of dendritic spines. To measure spine density, the number of spines per cell was then counted for 25 cells (50–100 μm total dendritic length per neuron). Significant differences were not observed between the control ($n = 42$ dendrites) and glutamate-treated dendrites ($n = 44$ dendrites; $p = 0.73$, Student's t test). Bar graphs represent dendritic spine density. The cumulative frequency plots in the bottom show distribution of spine length and spine width. The glutamate treatment significantly increased the spine length (control, 1.39 ± 0.03 μm, $n = 42$ dendrites; glutamate, 1.72 ± 0.05 μm, $n = 44$ dendrites, $p < 0.01$, Student's t test) and reduced the spine width (control, 0.96 ± 0.01 μm, $n = 42$ dendrites; glutamate, 0.82 ± 0.02 μm, $n = 44$ dendrites, $p < 0.01$, Student's t test). (**B**) Triple-labeled images of drebrin, F-actin and synapsin I in hippocampal neurons. Scale bars, 10 μm. (**C**) Bar graphs represent the density of synapsin I clusters. Synapsin I cluster density was measured according to previously described methods

(Takahashi et al., 2009). No significant differences in the density of synapsin I clusters were detected between control (n = 30 dendrites) and glutamate-stimulated neurons (n = 30 dendrites; p = 0.86, Student's t test). Data are presented as mean ± s.e.m.
(TIF)

Figure S2 Model for architectural changes in the actin cytoskeleton during LTP formation. (**A**) Dendritic spines in the resting state contain a dynamic F-actin pool (non-DA-actin) at the tip of the spine head, and a stable pool (DA-actin) in the base of the spine head. Although the dynamic F-actin pool shows quick treadmilling, polymerization and depolymerization of F-actin is balanced, consequently maintaining spine morphology. (**B**) Once Ca^{2+} enters through NMDA receptors, it activates myosin II ATPase through disinhibition of the DA-actin and myosin-II interaction. Consequently DA-actin exits the dendritic spine head and simultaneously monomeric actin refills the vacant space in the spine head. Both these changes cooperate to facilitate the polymerization of non-DA-actin, which is the predominant component of an enlargement F-actin pool in the spine head. Accordingly the spine head is enlarged. (**C**) Ca^{2+} reduction and/or APMA receptor activation induce DA-actin re-entry. The DA-actin re-entry reconstitutes the dynamic and stable F-actin pools in dendritic spines, contributing to maintenance of the enlarged spine morphology until the next DA-actin exodus is triggered.
(EPS)

Acknowledgments

We thank Drs. Kenji Hanamura and Mitsuyoshi Saito for helpful discussions and Ms. Tomoko Takahashi for technical assistance.

Author Contributions

Conceived and designed the experiments: TM YS TS. Performed the experiments: TM HY YI HT. Analyzed the data: TM YS HY YI HT NK MK. Wrote the paper: TM YS TS.

References

1. Shirao T, Kojima N, Nabeta Y, Obata K (1989) Two forms of drebrins, developmentally regulated brain proteins, in rat. Proc Japan Acad 65: 169–172.
2. Ishikawa R, Hayashi K, Shirao T, Xue Y, Takagi T, et al. (1994) Drebrin, a development-associated brain protein from rat embryo, causes the dissociation of tropomyosin from actin filaments. J Biol Chem 269: 29928–29933.
3. Aoki C, Sekino Y, Hanamura K, Fujisawa S, Mahadomrongkul V, et al. (2005) Drebrin A is a postsynaptic protein that localizes in vivo to the submembranous surface of dendritic sites forming excitatory synapses. J Comp Neurol 483: 383–402.
4. Grintsevich EE, Galkin VE, Orlova A, Ytterberg AJ, Mikati MM, et al. (2010) Mapping of drebrin binding site on F-actin. J Mol Biol 398: 542–554.
5. Sharma S, Grintsevich EE, Phillips ML, Reisler E, Gimzewski JK (2011) Atomic force microscopy reveals drebrin induced remodeling of f-actin with subnanometer resolution. Nano Lett 11: 825–827.
6. Asada H, Uyemura K, Shirao T (1994) Actin-binding protein, drebrin, accumulates in submembranous regions in parallel with neuronal differentiation. J Neurosci Res 38: 149–159.
7. Mizui T, Kojima N, Yamazaki H, Katayama M, Hanamura K, et al. (2009) Drebrin E is involved in the regulation of axonal growth through actin-myosin interactions. J Neurochem 109: 611–622.
8. Mikati MA, Grintsevich EE, Reisler E (2013) Drebrin-induced Stabilization of Actin Filaments. J Biol Chem 288: 19926–19938.
9. Takahashi H, Sekino Y, Tanaka S, Mizui T, Kishi S, et al. (2003) Drebrin-dependent actin clustering in dendritic filopodia governs synaptic targeting of postsynaptic density-95 and dendritic spine morphogenesis. J Neurosci 23: 6586–6595.
10. Worth DC, Daly CN, Geraldo S, Oozeer F, Gordon-Weeks PR (2013) Drebrin contains a cryptic F-actin-bundling activity regulated by Cdk5 phosphorylation. J Cell Biol 202: 793–806.
11. Honkura N, Matsuzaki M, Noguchi J, Ellis-Davies GC, Kasai H (2008) The subspine organization of actin fibers regulates the structure and plasticity of dendritic spines. Neuron 57: 719–729.
12. Shirao T, González-Billault C (2013) Actin filaments and microtubules in dendritic spines. J Neurochem 126: 155–164.
13. Sekino Y, Tanaka S, Hanamura K, Yamazaki H, Sasagawa Y, et al. (2006) Activation of N-methyl-D-aspartate receptor induces a shift of drebrin distribution: Disappearance from dendritic spines and appearance in dendritic shafts. Mol Cell Neurosci 31: 493–504.
14. Sekino Y, Kojima N, Shirao T (2007) Role of actin cytoskeleton in dendritic spine morphogenesis. Neurochem Int 51: 92–104.
15. Star EN, Kwiatkowski DJ, Murthy VN (2002) Rapid turnover of actin in dendritic spines and its regulation by activity. Nat Neurosci 5: 239–246.
16. Iki J, Inoue A, Bito H, Okabe S (2005) Bi-directional regulation of postsynaptic cortactin distribution by BDNF and NMDA receptor activity. Eur J Neurosci 22: 2985–2994.
17. Takahashi H, Yamazaki H, Hanamura K, Sekino Y, Shirao T (2009) AMPA receptor inhibition causes abnormal dendritic spines by destabilizing drebrin. J Cell Sci 122: 1211–1229.
18. Rex CS, Gavin CF, Rubio MD, Kramar EA, Chen LY, et al. (2010) Myosin IIb regulates actin dynamics during synaptic plasticity and memory formation. Neuron 67: 603–617.
19. Cheng XT, Hayashi K, Shirao T (2000) Non-muscle myosin IIB-like immunoreactivity is present at the drebrin-binding cytoskeleton in neurons. Neurosci Res 36: 167–173.
20. Hayashi K, Ishikawa R, Ye LH, He XL, Takata K, et al. (1996) Modulatory role of drebrin on the cytoskeleton within dendritic spines in the rat cerebral cortex. J Neurosci 16: 7161–7170.
21. Murrell MP, Gardel ML (2012) F-actin buckling coordinates contractility and severing in a biomimetic actomyosin cortex. Proc Natl Acad Sci USA 109: 20820–20825.
22. Lu W, Man H, Ju W, Trimble WS, MacDonald JF, et al. (2001) Activation of synaptic NMDA receptors induces membrane insertion of new AMPA receptors and LTP in cultured hippocampal neurons. Neuron 29: 243–254.
23. Shirao T, Obata K (1986) Immunochemical homology of 3 developmentally regulated brain proteins and their developmental change in neuronal distribution. Brain Res 394: 233–244.
24. Swayze RD, Lise MF, Levinson JN, Phillips A, El-Husseini A (2004) Modulation of dopamine mediated phosphorylation of AMPA receptors by PSD-95 and AKAP79/150. Neuropharmacology 47: 764–778.
25. Hayashi K, Shirao T (1999) Change in the shape of dendritic spines caused by overexpression of drebrin in cultured cortical neurons. J Neurosci 19: 3918–3925.
26. Xie H (1984) Differences in the Efficiency and Stability of Gene Expression after Transfection and Nuclear Injection: A Study with a Chick δ-Crystallin Gene. Cell Struct Funct 8: 315–325.
27. Hanamura K, Mizui T, Kakizaki T, Roppongi RT, Yamazaki H, et al. (2010) Low accumulation of drebrin at glutamatergic postsynaptic sites on GABAergic neurons, Neuroscience 169: 1489–1500.
28. Kaech S, Banker G (2006) Culturing hippocampal neurons, Nat Protoc 1: 2406–2415.
29. Xie Z, Srivastava DP, Photowala H, Kai L, Cahill ME, et al. (2007) Kalirin-7 controls activity-dependent structural and functional plasticity of dendritic spines. Neuron 56: 640–656.
30. Ryu J, Liu L, Wong TP, Wu DC, Burette A, et al. (2006) A critical role for myosin IIb in dendritic spine morphology and synaptic function. Neuron 49: 175–182.
31. Hardingham GE, Fukunaga Y, Bading H (2002) Extrasynaptic NMDARs oppose synaptic NMDARs by triggering CREB shut-off and cell death pathways. Nat Neurosci 5: 405–414.
32. Yuste R, Majewska A, Holthoff K (2000) From form to function: calcium compartmentalization in dendritic spines. Nat Neurosci 3: 653–659.
33. Matsumura F (2005) Regulation of myosin II during cytokinesis in higher eukaryotes. Trends Cell Biol 15: 371–377.
34. Matsuzaki M, Honkura N, Ellis-Davies GC, Kasai H (2004) Structural basis of long-term potentiation in single dendritic spines. Nature 429: 761–766.
35. Okamoto K, Nagai T, Miyawaki A, Hayashi Y (2004) Rapid and persistent modulation of actin dynamics regulates postsynaptic reorganization underlying bidirectional plasticity. Nat Neurosci 7: 1104–1112.
36. Korn ED, Carlier MF, Pantaloni D (1987) Actin polymerization and ATP hydrolysis. Science 238: 638–644.
37. Konishi M (1998) Cytoplasmic free concentrations of Ca^{2+} and Mg^{2+} in skeletal muscle fibers at rest and during contraction. Jpn J Physiol 48: 421–438.
38. Fukazawa Y, Saitoh Y, Ozawa F, Ohta Y, Mizuno K, et al. (2003) Hippocampal LTP is accompanied by enhanced F-actin content within the dendritic spine that is essential for late LTP maintenance in vivo. Neuron 38: 447–460.
39. Lynch MA (2004) Long-term potentiation and memory. Physiol Rev 84: 87–136.

Development/Plasticity/Repair

Microglia Enhance Neurogenesis and Oligodendrogenesis in the Early Postnatal Subventricular Zone

Yukari Shigemoto-Mogami,[1] Kazue Hoshikawa,[1] James E. Goldman,[2] Yuko Sekino,[1] and Kaoru Sato[1]

[1]Laboratory of Neuropharmacology, Division of Pharmacology, National Institute of Health Sciences, Tokyo 158-8501, Japan, and [2]Department of Pathology and Cell Biology, Columbia University College of Physicians and Surgeons, New York, New York 10032

Although microglia have long been considered as brain resident immune cells, increasing evidence suggests that they also have physiological roles in the development of the normal CNS. In this study, we found large numbers of activated microglia in the forebrain subventricular zone (SVZ) of the rat from P1 to P10. Pharmacological suppression of the activation, which produces a decrease in levels of a number of proinflammatory cytokines (i.e., IL-1β, IL-6, TNF-α, and IFN-γ) significantly inhibited neurogenesis and oligodendrogenesis in the SVZ. *In vitro* neurosphere assays reproduced the enhancement of neurogenesis and oligodendrogenesis by activated microglia and showed that the cytokines revealed the effects complementarily. These results suggest that activated microglia accumulate in the early postnatal SVZ and that they enhance neurogenesis and oligodendrogenesis via released cytokines.

Key words: cytokine; microglia; neurogenesis; neurosphere; oligodendrogenesis; subventricular zone

Introduction

CNS microglia have long been considered as resident immune cells, which are activated in response to pathological events. In pathological conditions, they change their morphology to an amoeboid shape, acquiring activation-specific phenotypes, such as chemotaxis, phagocytosis, and secretion of inflammatory cytokines (Nakajima and Kohsaka, 2001; Inoue, 2008; Monji et al., 2009; Kettenmann et al., 2011). However, microglia also have physiological roles in the normal CNS. They actively survey their territory with fine processes and receive stimuli from the environment as sensor cells (Kettenmann et al., 2011). *In vivo* lineage tracing studies have established that microglia differentiate from primitive myeloid progenitors that arise before embryonic day 8 and are identified in the CNS parenchyma even before definitive hematopoiesis (Ginhoux et al., 2010), whereas it has also been shown that microglia migrate from the lateral ventricle into the brain via the subventricular zone (SVZ) in the postnatal brain (Mohri et al., 2003). In the early embryonic brain, most microglia adopt an amoeboid morphology and characteristics of an activated form (Hirasawa et al., 2005). Microglia in the embryonic SVZ limit the production of cortical neurons by phagocytosing neural precursor cells (Cunningham et al., 2013). The number of microglia in the brain reaches a maximum during the early postnatal weeks (Wu et al., 1993; Xu and Ling, 1994), after which they transform into cells with a ramified shape, the typical morphology observed in the adult CNS (Ignácio et al., 2005). However, microglia are densely populated in neurogenic niches, such as the SVZ (Mosher et al., 2012), and appear more activated in the adult SVZ than in non-neurogenic zones (Goings et al., 2006). These developmental changes in the activation and the distribution of microglia strongly suggest that microglia play important roles in CNS development. However, the developmental dynamics of microglia in the postnatal SVZ and their roles in neurogenesis and gliogenesis at this stage are not well understood. We have examined the distribution and morphology of microglia in the rat forebrain during the neonatal-early postnatal period in detail and found a large number of active forms within the SVZ from P1 to P10, which then transformed from an activated form to a ramified form after P14. We here present evidence that microglia in the early postnatal SVZ promote both neurogenesis and oligodendrogenesis and that cytokines are important in these effects. To our knowledge, this is the first report showing a novel physiological function of microglia regulating neurogenesis and oligodendrogenesis in the early postnatal brain.

Received April 15, 2013; revised Dec. 21, 2013; accepted Dec. 27, 2013.

Author contributions: K.S. designed research; Y.S.-M., K.H., and K.S. performed research; Y.S.-M., K.H., J.E.G., Y.S., and K.S. analyzed data; Y.S.-M., J.E.G., Y.S., and K.S. wrote the paper.

This work was supported in part by a Grant-in-Aid for Young Scientists from MEXT, Japan (KAKENHI 21700422), the Program for Promotion of Fundamental Studies in Health Sciences of NIBIO, Japan, a Health and Labor Science Research Grant for Research on Risks of Chemicals, a Labor Science Research Grant for Research on New Drug Development from the MHLW, Japan to K.S., and a Health and Labor Science Research Grant for Research on Publicly Essential Drugs and Medical Devices, Japan to Y.S.

The authors declare no competing financial interests.

This article is freely available online through the *J Neurosci* Author Open Choice option.

Correspondence should be addressed to Dr. Kaoru Sato, Laboratory of Neuropharmacology, Division of Pharmacology, National Institute of Health Sciences, Kamiyoga 1-18-1, Setagaya-ku, Tokyo 158-8501, Japan. E-mail: kasato@nihs.go.jp.

DOI:10.1523/JNEUROSCI.1619-13.2014

 0270-6474/14/342231-13$15.00/0

Materials and Methods

Animals and treatment. All animals were treated in accordance with the guidelines for the Care and Use of Laboratory Animals of the Animal Research Committee of the National Institute of Health Sciences and followed the *Guide for the Care and Use of Laboratory Animals*. All experiments were approved by the Animal Research Committee of National Institute of Health Sciences and conformed to the relevant regulatory standards. The Wistar rats were purchased from Japan SLC and maintained under specific pathogen-free conditions at a controlled temperature and humidity and on a 12 h light/12 h dark cycle and had *ad libitum*

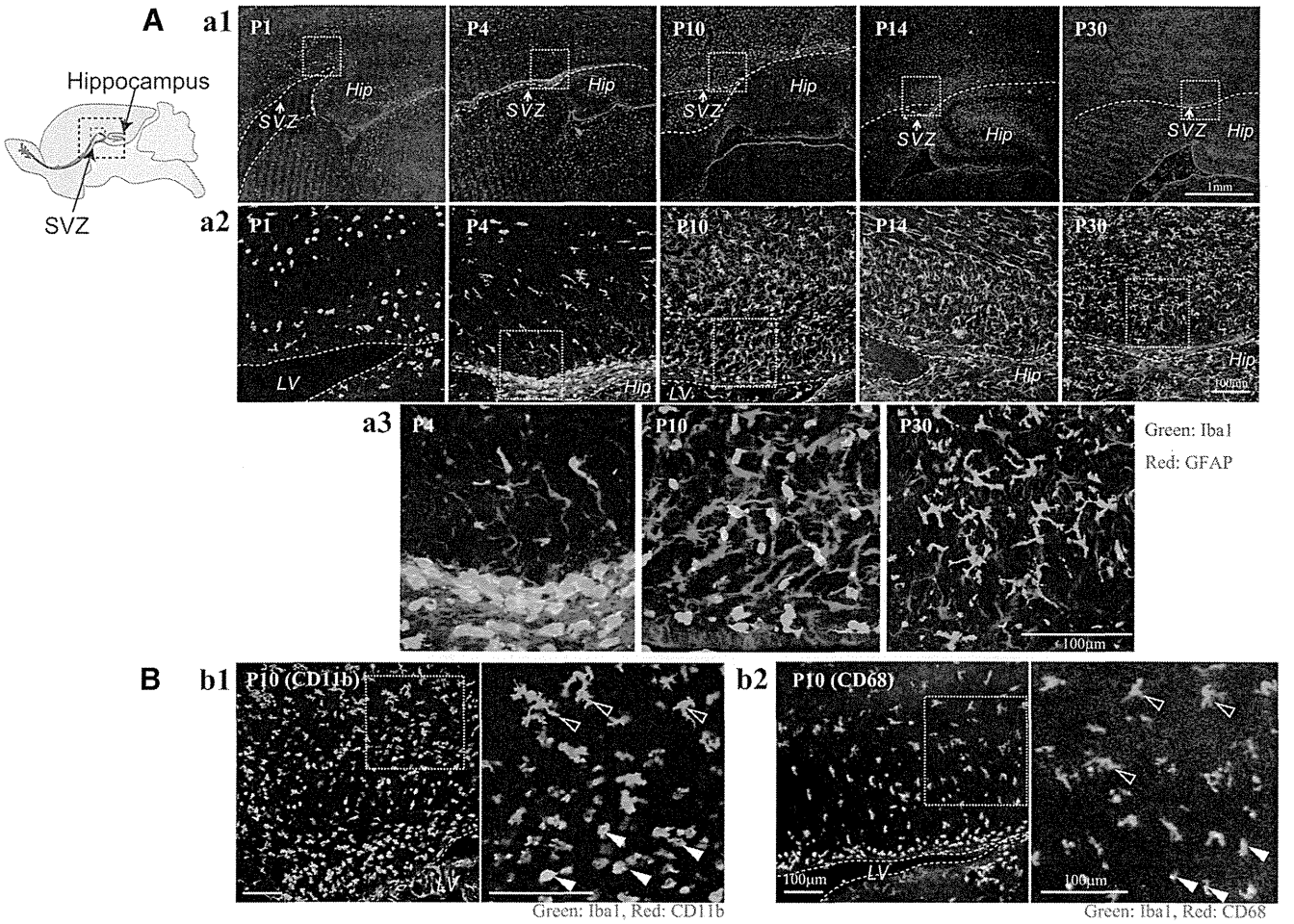

Figure 1. There is a population of activated microglia accumulated in the early postnatal SVZ. ***Aa1***, Distribution of microglia in the postnatal VZ/SVZ (P1, P4, P10, P14, P30). Sagittal sections of forebrains were immunostained with anti-Iba1 (green: microglia) and anti-GFAP antibodies (red: neural stem cells and astrocytes). ***Aa2***, Magnified images of the hatched squares in ***Aa1***. The accumulation in the SVZ in P4 and P10 was distinctive. ***Aa3***, Magnified images of the hatched squares in ***Aa2***. Morphological changes of microglia with age from amoeboid shape to more ramified shape is remarkable (P4, P10, P30). ***Bb1***, Activation of microglia in P10 SVZ. Sagittal sections immunostained with anti-CD11b (red: activated microglia) and anti-Iba1 antibodies (green: microglia). Right panel, Magnified image of the hatched square in the left panel. The microglia in the SVZ have an amoeboid shape and positive for CD11b (white arrowheads), whereas those outside SVZ have more ramified shape and are negative for CD11b (black arrowheads). ***Bb2***, Sagittal sections immunostained with anti-CD68 (red: activated microglia) and anti-Iba1 antibodies (green: microglia). Right panel, Magnified image of the hatched square in the left panel. The microglia in the SVZ have an amoeboid shape and positive for CD68 (white arrowheads), whereas those outside SVZ have more ramified shape and are negative for CD68 (black arrowheads). Similar results were obtained in three independent experiments.

access to food and water. Minocycline (30 mg/kg) or the same volume of PBS was injected into rats of either sex intraperitoneally for 3 d from postnatal day 2 (P2). Six hours after the last injection, rats were deeply anesthetized and the brains were removed on ice.

Immunohistochemistry (sagittal sections). Rats (P1, P4, P10, P14, P30) were anesthetized and then perfused with saline followed by 4% PFA, and then the brains were removed. From each half brain, sagittal sections were cut laterally at a thickness of 30 μm beginning 2 mm lateral from the midline. The sections were incubated for 2 h at room temperature in a blocking solution (3% normal goat serum, 0.3% Triton X-100 in PBS) and incubated for 24 h at 4°C in the solution, including the primary antibodies (rabbit anti-Iba1 antibody [019–9741, Wako; 1:500], mouse anti-GFAP antibody [MAB3402, Millipore; 1:200], mouse anti-rat CD11b antibody [MAB1405, AbD Serotec; 1:100], anti-rat CD68 antibody [MCA341R, AbD Serotec; 1:100], rabbit anti-Ki-67 [SP6, M3061, Spring Bioscience; 1:10], anti-nestin antibody [MAB353, Millipore; 1:100], goat anti-doublecortin [Dcx] antibody [sc-8066, Santa Cruz Biotechnology; 1:200], goat anti-PDGFRα antibody [sc-31178, Santa Cruz Biotechnology; 1:50], anti-oligodendrocyte marker O1 [O1] antibody [MAB344, Millipore, 1:50], mouse anti-MBP antibody [MAB 382, Millipore; 1:50], rabbit anti-ALDH1L1 antibody-astrocyte marker antibody [ab87117, Abcam; 1:1000], mouse anti-S100β antibody [S2532, Sigma; 1:100], rabbit anti IGF-1 antiserum [GroPep Biotechnology; [1:200]). After incubation, the sections were washed and incubated for 3 h at room temperature in the solution, including the secondary antibodies (anti-rabbit IgG-conjugated Alexa Fluorochrome or anti-mouse IgG-conjugated Alexa Fluorochrome [Invitrogen; 1:1000]). The stained sections were analyzed using a Nikon A1R-A1 confocal microscope system. To count the number of cells positive for each differentiation marker, 613 × 613 μm^2 and 1024 × 1024 μm^2 squares were set on both sides of the fornix. The cell numbers in the two squares were counted and averaged for the cell numbers in one section. The averaged data of 3 sections at 90 μm intervals were treated as the data of one animal and the data from 6 animals were statistically analyzed.

Immunohistochemistry (coronal sections). Three points on the skull at three different rostrocaudal stereotaxic coordinates (i.e., anterior, middle, posterior) were marked with animal tattoo ink (Ketchum) at P1. These three points with different rostrocaudal levels were determined according to a previous report (Suzuki and Goldman, 2003): rostral point: 2 mm anterior, 1 mm lateral to the bregma; middle point: 0.7 mm anterior, 1 mm lateral to the bregma; caudal point: 0.5 mm posterior, 1 mm lateral to the bregma. Then the animals were perfused at P1, P3, P10, and P30, and the brains were removed as described above. From each half brain, coronal sections were cut at each marked point from anterior to posterior. The sections were immunostained with anti-Iba1 and anti-CD68 as described above. After immunostaining, the sections were coun-

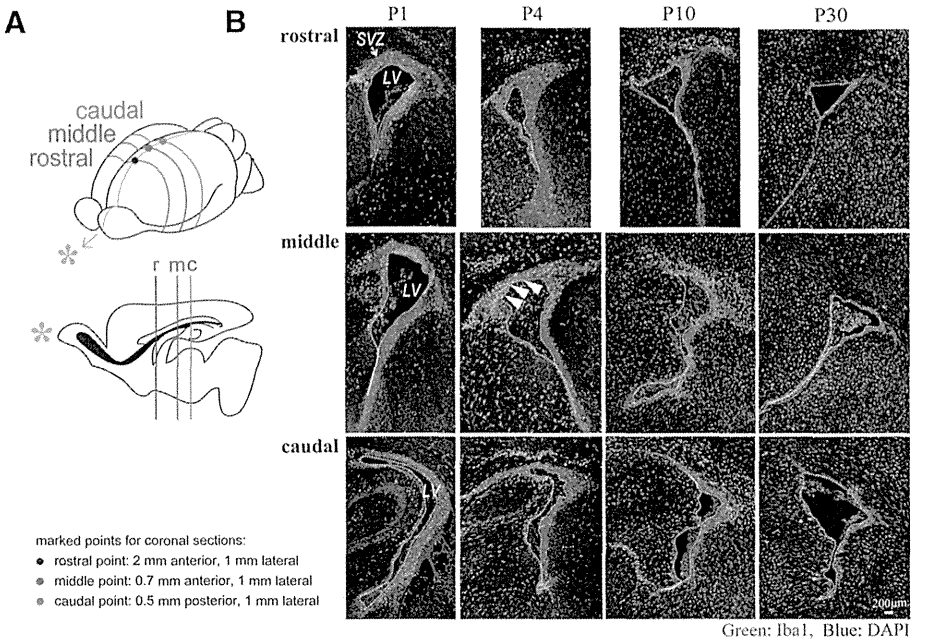
A
B
caudal
middle
rostral
r mc
P1
P4
P10
P30
rostral
middle
caudal
SVZ
LV
marked points for coronal sections:
rostral point: 2 mm anterior, 1 mm lateral
middle point: 0.7 mm anterior, 1 mm lateral
caudal point: 0.5 mm posterior, 1 mm lateral
200μm
Green: Iba1, Blue: DAPI

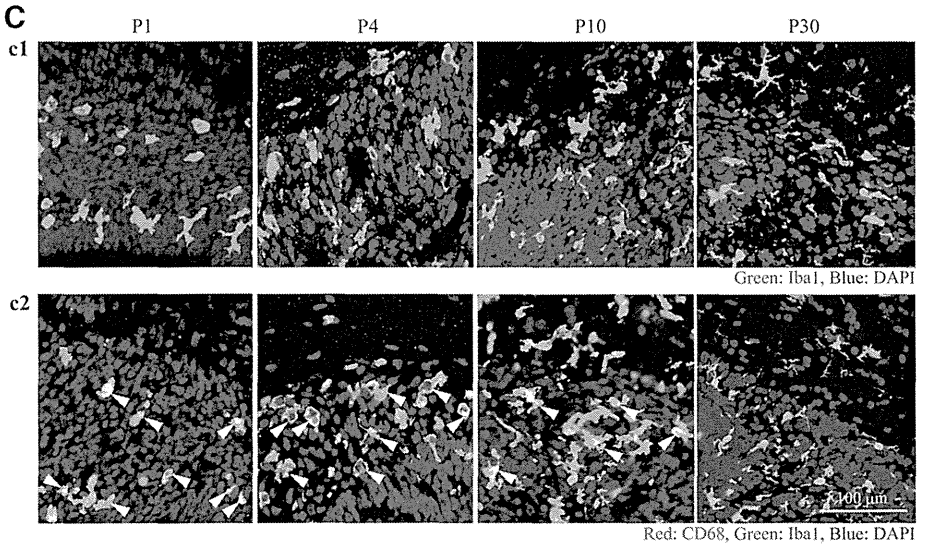
C
c1
P1
P4
P10
P30
Green: Iba1, Blue: DAPI
c2
100 μm
Red: CD68, Green: Iba1, Blue: DAPI

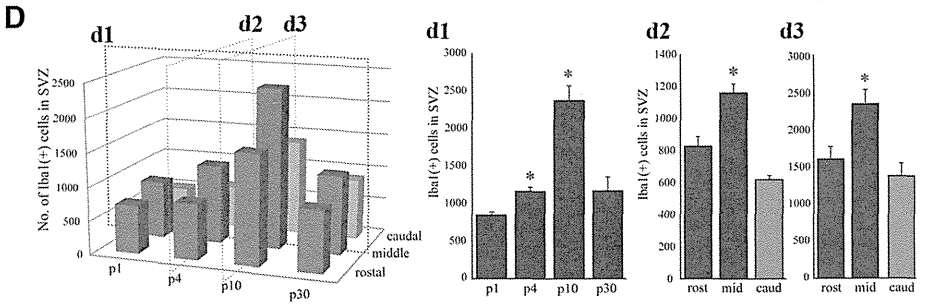
D
d1
d2
d3
No. of Iba1(+) cells in SVZ
caudal
middle
rostral
p1
p4
p10
p30
Iba1(+) cells in SVZ
rost
mid
caud

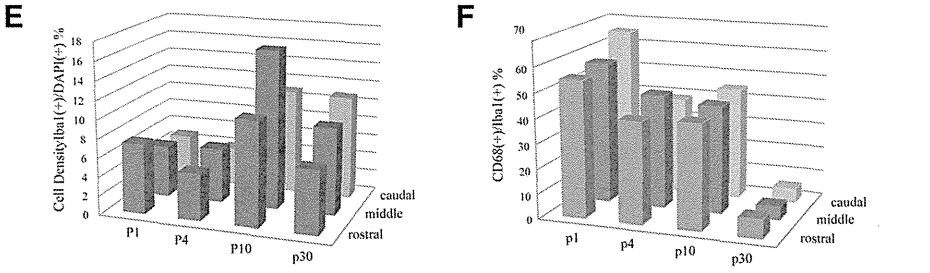
E
Cell Density:Iba1(+)/DAPI(+) %
caudal
middle
rostral
P1
P4
P10
p30
F
CD68(+)/Iba1(+) %
p1
p4
p10
p30

terstained with DAPI (1:500; Invitrogen) for 30 min to visualize the SVZ. The cell numbers of microglia (Iba1 $^+$) and activated microglia (Iba1 $^+$ CD68 $^+$) in the SVZ (the region with dense DAPI signals) were counted in one section. The averaged data of three sections at 90 μm intervals across the marked points were treated as the data for each rostrocaudal level. The data from 6 to 9 hemispheres per one rostrocaudal level were statistically analyzed.

Western blotting. P4 Wistar rat brains were cut into sagittal sections. Under a microscope, a parasagittal section (from 1 mm lateral, 2 mm thickness) was taken from each half brain and meninges were carefully removed. The VZ/SVZ was identified by its slightly darker, more transparent appearance compared with the overlying corpus callosum. We cut out the VZ/SVZ between 0.4 mm anterior and 3 mm posterior (posterior end of SVZ) from bregma so as not to include the rostral migratory stream. Dissected VZ/SVZ tissues were homogenized on ice in extraction buffer (20 mM Tris, 2 mM EDTA, 0.5 mM EGTA, 0.32 M sucrose, protease inhibitor mixture), and centrifuged at 1000 × *g* for 10 min. Proteins in the lysates were resolved with SDS-PAGE and transferred to PVDF membranes. The membranes were incubated overnight in BlockAce blocking solution at 4°C. Then the membranes were incubated with primary antibodies (anti-CD11b [1:1000], anti-CD68 [1:2000], anti-nestin [1:1000], anti-PDGFRα [1:200], anti-ALDH1L1 [1:1000], anti-S100β [1:2000]) for 1 h at 25°C. After washing three times, the membranes were incubated with HRP-conjugated anti-rabbit or anti-mouse antibody (1:5000) for 1 h at 25°C. The membranes were then washed three times and signals were visualized by chemiluminescence detectors LAS3000 (Fuji film).

Measurement of cytokine levels. Cytokine levels in the SVZ were determined with Bio-Plex cytokine analysis system (Bio-Rad Laboratories). Tissue lysates of VZ/SVZ fractions were obtained from rats at P1, P4, P10, and P30 as described in Western blotting. The concentrations of Il-1α, Il-1β, IL-2, IL-4, IL-6, Il-10, GM-CSF, IFN-γ, and TNF-α were measured by the Bio-Plex rat cytokine 9 plex kit according to the manufacturer's instruction. In some cases, IGF-1, Il-1β IL-6, TNF-α, and IFN-γ concentrations were measured by ELISA kit according to the manufacturer's instruction. The protein levels of tissue lysates were measured by BCA protein assay. The amount of each cytokine in 100 μg of total protein is shown for comparison. To determine the cytokine release from activated microglia *in vitro*, microglia were activated by LPS (10 ng/ml) in the presence or absence of minocycline (10 μM) for 30 min and washed carefully and incubated in the normal medium for 24 h. After 24 h incubation, the cell culture supernatants were collected, and concentration of Il-1β, IL-6, IFN-γ, and TNF-α were measured by ELISA kit.

Cell culture: neurosphere culture. Rat neural stem cells were cultured as previously described (Reynolds et al., 1992; Hamanoue et al., 2009) with slight modifications. Briefly, telencephalons were dissected from embryonic day 16 (E16) rats of either sex in ice-cold DMEM/F12, minced, and dispersed into single cells by pipetting. Cells were then cultured in DMEM/F12 containing B27 supplement (×200), 20 ng/ml FGF2, and 20 ng/ml EGF for 7 d. The primary neurospheres and single cells were differentiated in growth factor-free medium in glass chambers coated with ornithine/fibronectin. In some cases, primary neurosphere were incubated with TrypLE Select for 15 min and dissociated by pipetting. Single cells were differentiated in glass chambers coated with polyornithine/laminin.

Microglia culture. Rat microglia were cultured as previously described (Nakajima et al., 1992). In brief, mixed glial cultures were prepared from the cerebral cortex of P1 Wistar rats and maintained for 12–23 d in DMEM containing 10% FBS. The floating microglia over the mixed glial cultures were collected and transferred to appropriate dishes or transwells.

Neural stem cell differentiation assay. To examine the effects of activated microglia on neural development and the contribution of cytokines to the effects, we used modified cocultures of neurospheres with activated microglia. Microglia cultured independently of neurospheres on transwells were activated by LPS (10 ng/ml) in the presence or absence of minocycline (10 μM) for 30 min and washed carefully to prevent residual LPS and minocycline. The transwells on which microglia were cultured were set on the neurospheres 1 d after the starting point of the differentiation and incubated for differentiation periods suitable for neurons (7 d) or oligodendrocytes (11 d). In some cases, we performed the coculture of cells dissociated from neurospheres and activated microglia. To check the effects of minocycline alone, these cells were incubated in the presence of minocycline (10 μM) for 7 d. Neurospheres and single neural stem cells were immunohistochemically stained for β3-tubulin, PDGFRα, O4, GFAP, and TOTO3 according to the manufacture's instruction (Stem Cell Kits, R&D Systems). To examine the effects of function-blocking antibodies on differentiation, the neurospheres were differentiated in the presence of function-blocking antibodies (goat anti-rat IL-1β antibody [AF-501-NA, R&D Systems], goat anti-rat IL-6 antibody [AF-506, R&D Systems], TNF-α antibody [70R-TR007X, Fitzgerald], and goat anti-mouse/rat IFN-γ antibody [AF-585-NA, R&D Systems]) (1 μg/ml for each). The effects of these function-blocking antibodies were compared with the same concentration of isotype-matched control IgG: normal goat IgG control [AB-108-C, R&D Systems] and rabbit IgG control [31R-AR001, R&D Systems] (1 μg/ml for each). The effect of the mixture of function blocking antibodies (goat anti-rat IL-1β antibody, goat anti-rat IL-6 antibody, TNF-α antibody, and goat anti-mouse/rat IFN-γ antibody, 1 μg/ml for each) was compared with the control, which included same concentrations of isotype-matched control IgGs (i.e., 3 μg/ml of normal goat IgG control and 1 μg/ml of rabbit IgG control). To examine the effects of a single cytokine, the neurospheres were differentiated in the presence of each individual recombinant cytokine (rIL-1β, rIL-6, rTNF-α, and rIFN-γ at 1 or 10 ng/ml). After the differentiation period, the cells were stained immunocytochemically as described above.

Data analysis and statistics. All data are shown as the mean ± SEM. Statistical analysis was performed using Student's *t* test, or Tukey's test by ANOVA. Differences were considered to be significant at $p < 0.05$.

Materials. Minocycline, LPS, anti-S100β antibody (S2532), and EGF were purchased from Sigma. Bio-Plex rat cytokine 9 plex was purchased from Bio-Rad Laboratories. Recombinant cytokines (rIL-1β, rIL-4, rIL-6, rIFN-γ, rTNF-α) and FGF2 were purchased from PeproTech. Maximum sensitivity substrate and BCA protein assay were purchased from Thermo Scientific. CanGet Signals was purchased from Toyobo. HRP-conjugated anti-rabbit, mouse antibodies were purchased from GE Healthcare Life Science. DAPI, TOTO3, anti-mouse, sheep, rabbit IgG, and anti-mouse IgM-conjugated AlexaFluor were purchased from Invitrogen. BlockAce was purchased from DS Pharma Biomedical. B27 supplement, TrypLE Serect, FBS, and DMEM were purchased from Invitrogen.

Results

We first investigated the distribution of microglia in the postnatal rat forebrain (Figs. 1 and 2). Sagittal sections were immuno-

←

Figure 2. The temporal and spatial dynamics of activated microglia in the postnatal SVZ. ***A***, A schematic of the rostrocaudal levels in this experiment. ***B***, The distribution of microglia in the rostral, medial, and caudal SVZ at P1, P4, P10, and P30. Coronal sections of forebrains at rostral (2 mm anterior to the bregma), medial (0.7 mm anterior to the bregma), and caudal (0.5 mm posterior to the bregma) levels were immunostained with anti-Iba1 (green: microglia) followed by DAPI staining (blue: cell nuclei). A population of activated microglia accumulated within the SVZ at P1-P10. ***Cc1***, Typical morphology of microglia in the middle SVZ at P1, P4, P10, and P30. Morphological change of microglia with age from amoeboid shape to more ramified shape is remarkable. ***Cc2***, The middle SVZ sections immunostained with anti-CD68 (red: activated microglia) and anti-Iba1 antibodies (green: microglia). The microglia at P1, P4, and P10 in the SVZ have an amoeboid shape and are positive for CD68 (representative cells: white arrowheads), whereas those at p30 have a more ramified shape and are negative for CD68. ***D***, The quantification of the number of Iba1 $^+$ cells in the SVZ. ***d1***, Time course of the Iba1 $^+$ microglia in the middle SVZ. The number peaked at P10. d2, d3, The comparison of the numbers of microglia among the rostral, middle, and caudal SVZ at P4 (***d2***) and P10 (***d3***). *$p < 0.05$ versus p1 or rost group (Tukey's test by ANOVA). Data are mean ± SEM. ***E***, The cell density of Iba1 $^+$ microglia at different rostrocaudal levels at P1, P4, P10, and P30. The cell density of microglia in the SVZ paralleled with that of the number of microglia throughout a period of the observation. ***F***, The ratio of activated microglia in the SVZ (CD68 $^+$/Iba1 $^+$). During the experimental period, the highest ratio was obtained at P1. We confirmed the similar results in three independent experiments.

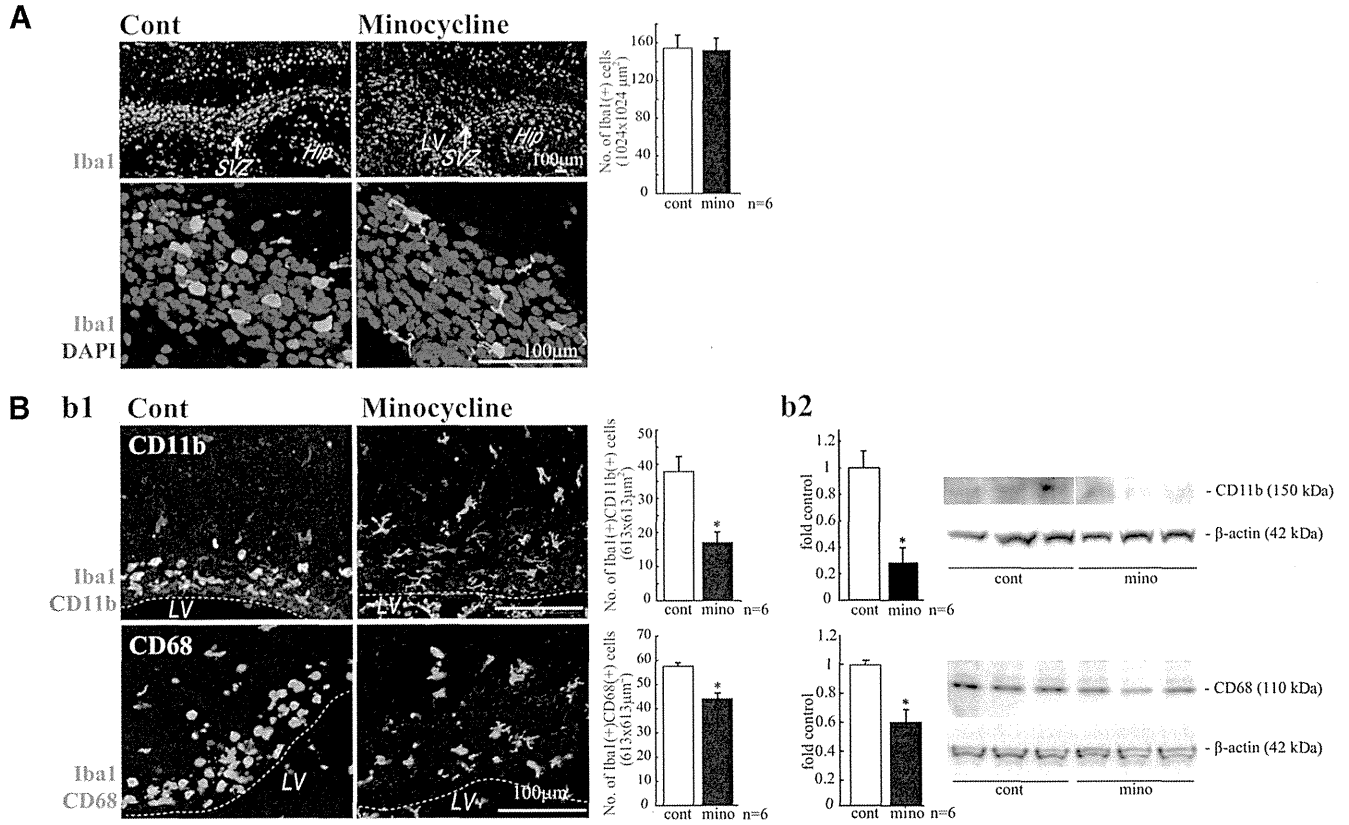

Figure 3. Minocycline suppressed microglial activation *in vivo*. ***A***, Effects of minocycline on the number of Iba1 $^{+}$ cells in the SVZ and their morphologies. Minocycline was administered by intraperitoneal injection for 3 d beginning at P2 (30 mg/kg/d, P2-P4, $n = 6$/group). Sagittal sections of minocycline-treated forebrains were immunostained for Iba1 (green) followed by DAPI staining (cyan). Although the number of Iba1 $^{+}$ microglia in the SVZ did not change (graph), their shape shifted from an amoeboid type to a more ramified type by minocycline (bottom). ***Bb1***, Effects of minocycline on the expression of activation markers and the morphologies of microglia. Sagittal sections of minocycline-treated forebrains were immunostained for Iba1 (green), and CD11b (red), and CD68 (red). Minocycline significantly decreased the number of cells positive for CD11b or CD68. The morphologies of the cells were also changed from amoeboid shape to more ramified shape. ***Bb2***, The significant decrease in the expression of CD11b and CD68 was confirmed by Western blotting of the SVZ as well. $^{*}p < 0.05$ (Student's t test). Data are mean ± SEM. Similar results were obtained in three independent experiments.

stained with anti-Iba1, the marker for all microglia (green: microglia), and anti-GFAP antibodies (red: neural stem cells and astrocytes) at P1, P4, P10, P14, and P30. We found that a large number of microglia accumulated in the postnatal SVZ from P1 to P10 (Fig. 1*A*), especially at P4. The microglia in the VZ/SVZ at P1 and P4 display an amoeboid shape, whereas those outside the SVZ have a more ramified shape (Fig. 1*Aa2*). At P10, the number of microglia outside the SVZ had dramatically increased; the microglia in the VZ/SVZ remained amoeboid. At P14, the number of microglia had increased further and now ramified microglia were also observed in the VZ/SVZ. At P30, the numbers of microglia in the SVZ had decreased and most of the microglia had assumed a ramified shape. Further magnified images in Figure 1*Aa3* show that the shape of microglia in the SVZ changed gradually from amoeboid (P4) to ramified (P30). Figure 1*B* shows the expression of CD11b (Fig. 1*Bb1*) and CD68 (Fig. 1*Bb2*) in the SVZ microglia at P10. CD11b is potentially a marker for all microglia; however, its level is highly elevated by activation. CD68 is a marker for activated microglia. The levels of CD11b and CD68 are much higher in the amoeboid microglia in the SVZ (white arrowheads) than in the ramified ones outside the SVZ (black arrowheads), indicating that the SVZ amoeboid microglia have an activated phenotype.

To examine the developmental dynamics of microglia in the SVZ temporally and spatially, we examined the distribution of microglia in coronal sections that include rostral, medial, and caudal SVZ at P1, P4, P10, and P30 (Fig. 2). Each rostrocaudal level was determined according to a previous report (Suzuki and Goldman, 2003). Coronal sections were immunostained with anti-Iba1 (green: microglia) followed by DAPI staining (blue: cell nuclei) (Fig. 2*B*,*C*). The SVZ could be clearly delineated by its dense cellularity. From P1 to P10, a large number of microglia accumulated at all rostral, middle, and caudal levels. When we quantified the number of microglia in the SVZ, they gradually increased from P1 to P10, reached a maximum at p10, and decreased at P30 at all coronal levels (Fig. 2*B*,*D*, d1). Microglia displayed an amoeboid shape at P1, P4, and P10 but had become more ramified at P30 (Fig. 2*Cc1*). Among the different rostrocaudal levels, the number of microglia in the middle SVZ was significantly larger than in other levels at all ages (Fig. 2*D*, d2, d3). The changes in cell density (i.e., the ratio of Iba1 $^{+}$/DAPI $^{+}$) of microglia in the SVZ paralleled that of the number of microglia throughout the period of observation (Fig. 2*E*). We next examined immunostaining for CD68 in SVZ microglia. Figure 2*Cc2* shows representative images of double staining with anti-Iba1 and anti-CD68. At P1 and P4, most Iba1+ microglia in the SVZ were also positive for CD68. At P4, the CD68 signals became much stronger. At P10, a few microglia had appeared that had little CD68. At P30, double-positive cells were markedly decreased in number. The time course of the ratio of CD68 $^{+}$/Iba1 $^{+}$ cells is shown in Figure 2*F*: the highest ratio was obtained at P1. The ratios at P4 and P10 were almost equivalent and then were

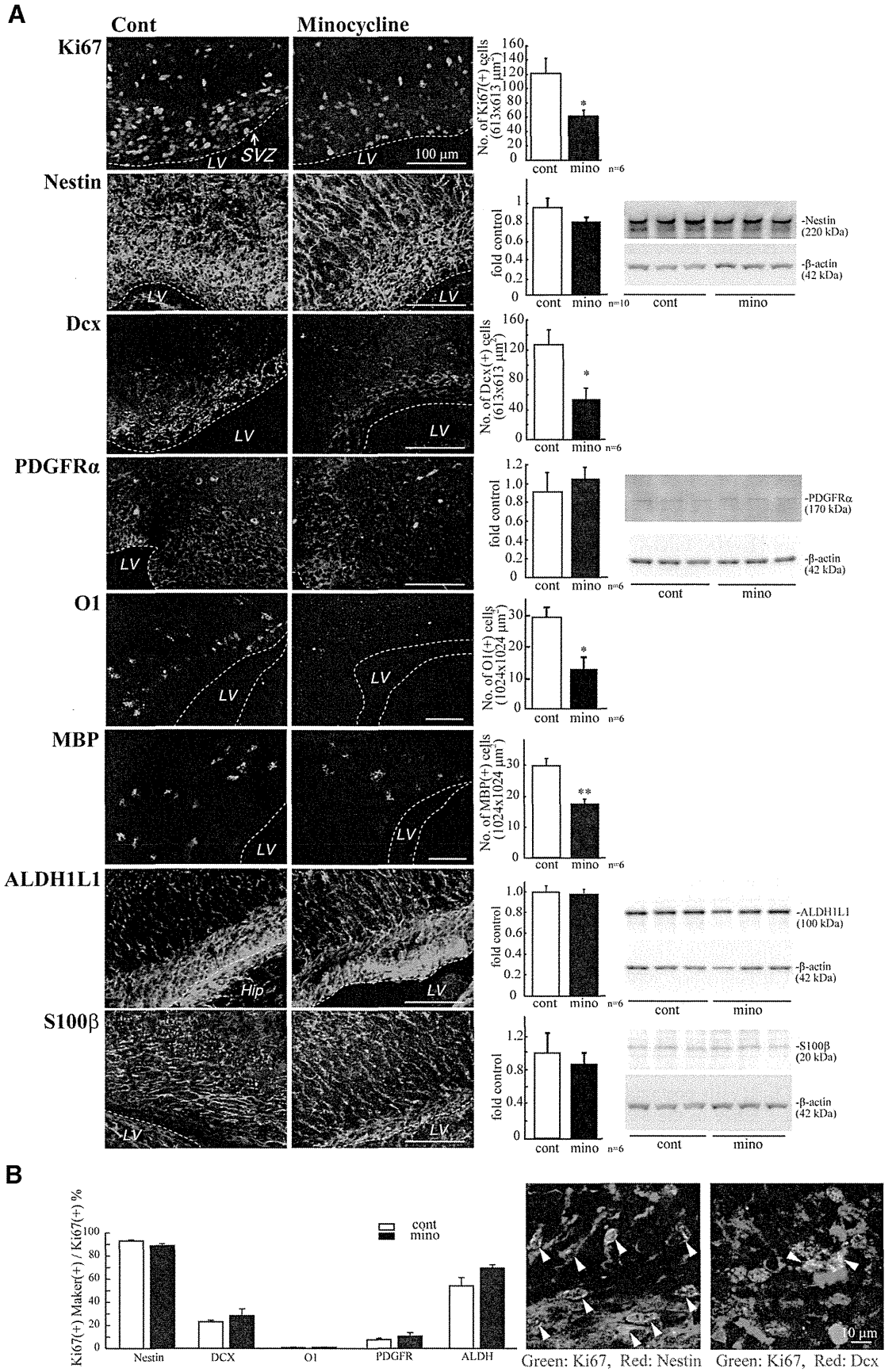

Figure 4. Minocycline decreased the numbers of proliferating cells, neuronal progenitors, and oligodendrocyte progenitors in the early postnatal SVZ. ***A***, Minocycline was administered by intraperitoneal injection for 3 d beginning at P2 (30 mg/kg/d, P2-P4, $n = 6$/group). Sagittal sections of forebrains were immunostained with antibodies to Ki67, nestin, Dcx, PDGFRα, O1, MBP, ALDH1L1, and S100β. The numbers of cells positive for Ki67, Dcx, MBP, or O1 were counted, whereas the protein levels of nestin, PDGFRα, ALDH1L1, and S100β (*Figure legend continues.*)

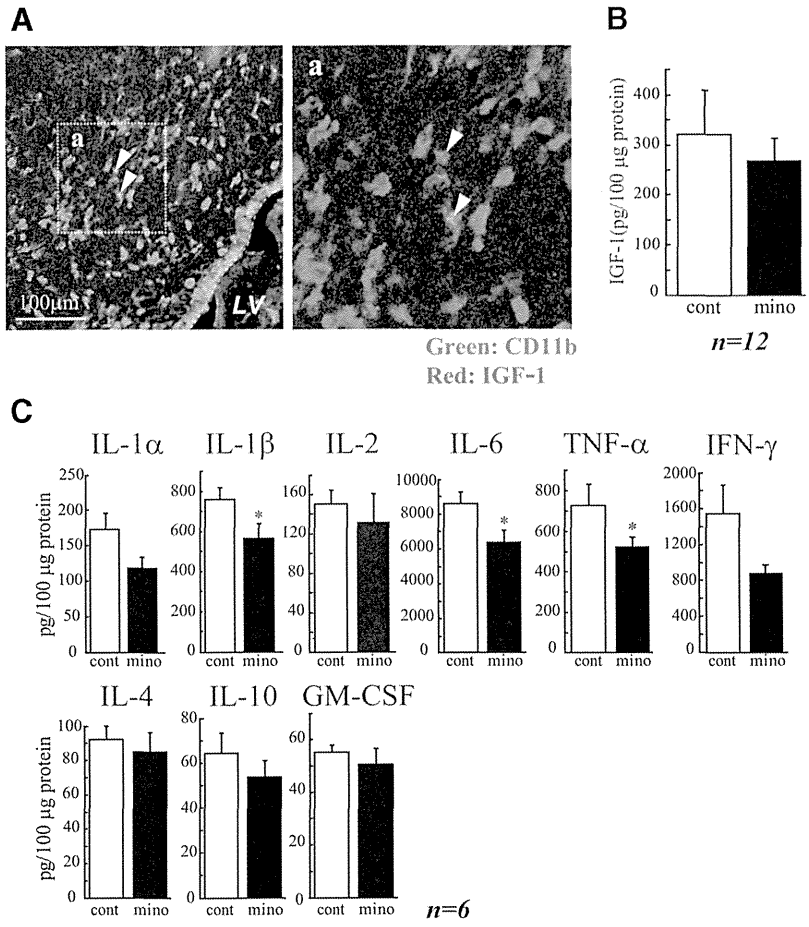

Figure 5. The activated microglia raised the cytokine levels in the SVZ. ***A***, A subpopulation of the microglia express IGF-1 in the early postnatal SVZ, but IGF-1 is not involved in the action of activated microglia during this period. Sagittal sections were immunostained with anti-CD11b (green: microglia) and anti IGF-1 (red) antibodies. Right panel, Magnified image of the square in the left. A subpopulation of microglia is positive for IGF-1 (arrowheads). The percentage of CD11b $^+$IGF-1 $^+$ was 43.42 ± 6.72% in CD11b $^+$ cells. ***B***, Minocycline did not affect the amount of IGF-1 in the early postnatal SVZ. Minocycline was administered by intraperitoneal injection for 3 d beginning at P2 (30 mg/kg/d, P2-P4, n = 6/group), and the amount of IGF-1 in the SVZ was quantified by ELISA. ***C***, Minocycline decreased the amount of inflammatory cytokines in the SVZ. IL-1α, IL-1β, IL-2, IL-4, IL-6, IL-10, GM-CSF, IFN-γ, and TNF-α levels in the SVZ tissue lysate were measured by BioPlex cytokine detection assay system. *$p <$ 0.05 (Student's t test). n = 6 rats/group. Data are mean ± SEM. Similar results were obtained in two independent experiments.

remarkably decreased at P30. These results are consistent with those obtained from the sagittal sections (Fig. 1), showing the population of activated microglia that accumulated within the SVZ during the early postnatal period.

We therefore examined the specific roles of these microglia in the early postnatal SVZ. At early postnatal ages, both neurogenesis and gliogenesis are active in the SVZ (Gould et al., 1999; Wagner et al., 1999; Doetsch and Scharff, 2001; Zerlin et al., 2004; Marshall et al., 2008). To suppress the activation of microglia, we used minocycline, a tetracycline antibiotic, long used to suppress microglial activation (Tikka et al., 2001; Zhao et al., 2007). We first verified the effects of minocycline on the activation of microglia. Minocycline was administered by intraperitoneal injection for 3 d beginning at P2 (30 mg/kg/d, P2-P4, n = 6/group), and sagittal sections of minocycline-treated rat forebrains were immunostained for Iba1, CD11b, and CD68. Minocycline did not change the numbers of Iba1-positive microglia in the VZ/SVZ (Fig. 3*A*, top), but it dramatically changed their shape from amoeboid to more ramified (Fig. 3*A*, bottom). The number of CD11b $^+$ cells was significantly decreased (Fig. 3*Bb1*, top and graph), and the decrease in CD11b levels in the SVZ was confirmed by Western blotting (Fig. 3*Bb2*, top graph and photo). The number of CD68 $^+$ cells and the level of CD68 were also decreased (Fig. 3*B*, bottom data). These results indicate that our administration of minocycline suppresses the activation of SVZ microglia.

We then investigated the effects of minocycline on early postnatal differentiation. After the administration of minocycline, sagittal sections were immunostained with differentiation markers: Ki67 (proliferating cells), nestin (stem cells), Dcx (neuronal progenitors), PDGFRα (oligodendrocyte progenitors [polydendrocytes]), O1 (oligodendrocyte progenitors [premyelinating oligodendrocytes]), MBP (mature oligodendrocyte [premyelinating and myelinating oligodendrocytes] (Nishiyama et al., 2009), ALDH1L1 (astrocyte progenitors), and S100β $^+$ (astrocytes) (Fig. 4*A*). The numbers of cells positive for Ki67, Dcx, O1, and MBP were counted, whereas the levels of nestin, PDGFα, ALDH1L1, and S100β were examined by Western blotting because it was hard to discriminate the cell morphologies by these signals. Minocycline significantly decreased the number of Ki67 $^+$ cells and slightly decreased the level of nestin. The number of cells positive for Dcx was also significantly reduced. Furthermore, minocycline decreased the numbers of cells positive for O1 and MBP, whereas the numbers of PDGFRα $^+$ cells rather tended to increase. The levels of ALDH1L1 and S100β did not change. These results suggest that activated microglia in the early postnatal SVZ enhance neurogenesis and oligodendrogenesis, and activated microglia affect oligodendrocyte progenitors at rather later stage of differentiation. We also performed the double staining of Ki67 with the respective differentiation markers (Fig. 4*B*). Although the total number of Ki67 $^+$ cells was decreased by minocycline, consistent with Figure 4*A*, the percentage of Ki67 $^+$ cells also positive for the respective differentiation markers did not change in the absence or presence of minocycline (Fig. 4*B*, left graph), suggesting that minocycline did not affect the proliferation of progenitors of the specific cell types. Typical images of the SVZ cells positive for

←

(*Figure legend continued.*) were examined by Western blotting. Minocycline significantly decreased the number of Ki67 $^+$ proliferating cells and decreased the level of nestin. The number of cells positive for Dcx was significantly reduced. Minocycline decreased the numbers of cells positive for O1 and MBP, whereas the expression level of PDGFRα tended to increase. *$p <$ 0.05, **$p <$ 0.01 (Student's t test). n = 6 mice/group. Data are mean ± SEM. ***B***, The ratio of the Ki67 $^+$ cells also positive for respective differentiation markers did not change in the absence or presence of minocycline (left graph). Typical images of the cells positive for Ki67 and Nestin, and the cells positive for Ki67 and Dcx in the control group are shown (right panels). We confirmed the same results in three independent experiments.

Ki67 and Nestin, and the cells positive for Ki67 and Dcx in the control group are shown (Fig. 4*B*, right panels).

Butovsky et al. (2006a) have reported that IGF-1 released from activated microglia promoted neurogenesis and oligodendrogenesis from adult stem/progenitor cells. We examined whether microglia in the early postnatal SVZ produce IGF-1 (Fig. 5*A*). Microglia did contain IGF-1 protein, but the percentage of $CD11b^+$ cells also positive for $IGF\text{-}1^+$ was 43.42 ± 6.72%. Furthermore, the amount of IGF-1 in the SVZ tissue lysates was not decreased by minocycline (Fig. 5*B*). These results suggest that, although a fraction of activated microglia in the early postnatal SVZ did produce IGF-1, the effects of activated microglia on neurogenesis and oligodendrogenesis obtained in our study were independent of IGF-1. Activated microglia release a number of cytokines. In some cases other than pathological conditions, cytokines also have physiological roles (Schäfers and Sorkin, 2008; Spedding and Gressens, 2008; Camacho-Arroyo et al., 2009; Miller et al., 2009; Spooren et al., 2011). We therefore investigated whether the SVZ microglia cause the increase in cytokine concentrations in the early postnatal SVZ (Fig. 5*C*). We examined the effects of minocycline on the levels of IL-1α, IL-1β, IL-2, IL-4, IL-6, IL-10, GM-CSF, IFN-γ, and TNF-α. To measure multiple cytokines in a small volume of tissue samples simultaneously, we used the BioPlex cytokine detection assay system (Bio-Rad). The levels of IL-1β, IL-6, and TNF-α were significantly decreased by the 3-day intraperitoneal administration of minocycline (Fig. 5*C*). Although the difference was not significant, the level of IFN-γ also tended to be decreased.

To examine more directly whether these cytokines affected neurogenesis and oligodendrogenesis, we performed *in vitro* experiments, coculturing neural stem cells with activated microglia. Microglia cultured independently of neurospheres on transwells were activated by LPS (10 ng/ml, 30 min) in the presence or absence of minocycline (10 μM). The microglia were carefully washed to remove residual LPS and minocycline, and then the transwell on which microglia were cultured was set onto the neurosphere cultures in prodifferentiation conditions. The activated microglia significantly increased the number of $\beta3\text{-tubulin}^+$ and $O4^+$ cells but had no effects on $GFAP^+$ cells in neurospheres (Fig. 6*A*,*B*). Minocycline almost completely suppressed the effects of activated microglia on the numbers of cells positive

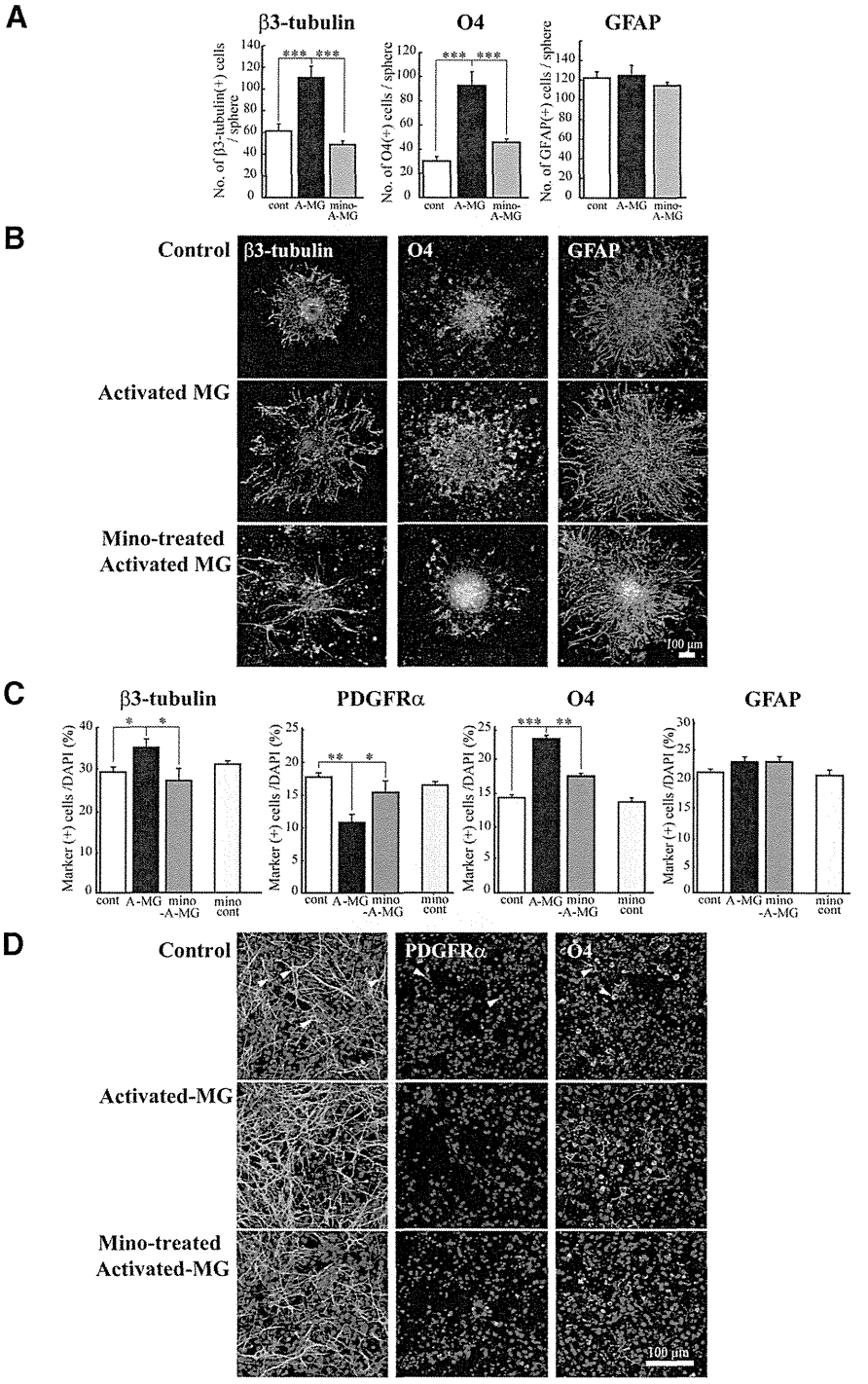

Figure 6. The reproduction of the enhancement of neurogenesis and oligodendrogenesis by activated microglia *in vitro*. Microglia cultured independently of neurosphere on transwells were activated by LPS (10 ng/ml, 30 min) in the presence or absence of minocycline (10 μM), washed carefully, and the transwells were set onto the neurospheres or dissociated cells from neurosphere in prodifferentiation conditions. After differentiation periods suitable for neurons (7 d) or oligodendrocytes (11 d), neurospheres were stained for β3-tubulin (green), PDGFRα (green), O4 (green), GFAP (red), and TOTO3 (cyan). To check the effects of minocycline alone, dissociated cells were incubated in the presence of minocycline (10 μM) for 7 d. ***A***, Quantification of the numbers of neurons, oligodendrocyte progenitors, or astrocytes differentiated from neurospheres cocultured with activated microglia in the presence or absence of minocycline. $^{***}p < 0.001$ (Tukey's test by ANOVA). $n = 12$ neurospheres/group. Data are mean ± SEM. ***B***, Representative immunostained images of neurospheres cocultured with activated microglia in the presence or absence of minocycline. ***C***, The effects of activated microglia on differentiation of single cells dissociated from neurospheres in the presence or absence of minocycline. The effects of minocycline alone were also shown (mino-cont in each graph). $^{*}p < 0.05$, $^{**}p < 0.01$, $^{***}p < 0.001$. (Tukey's test by ANOVA). $n = 12$ neurospheres/group. Data are mean ± SEM. ***D***, Images of cells immunostained for differentiation markers. Arrowheads indicate the representative cells positive for the differentiation markers.

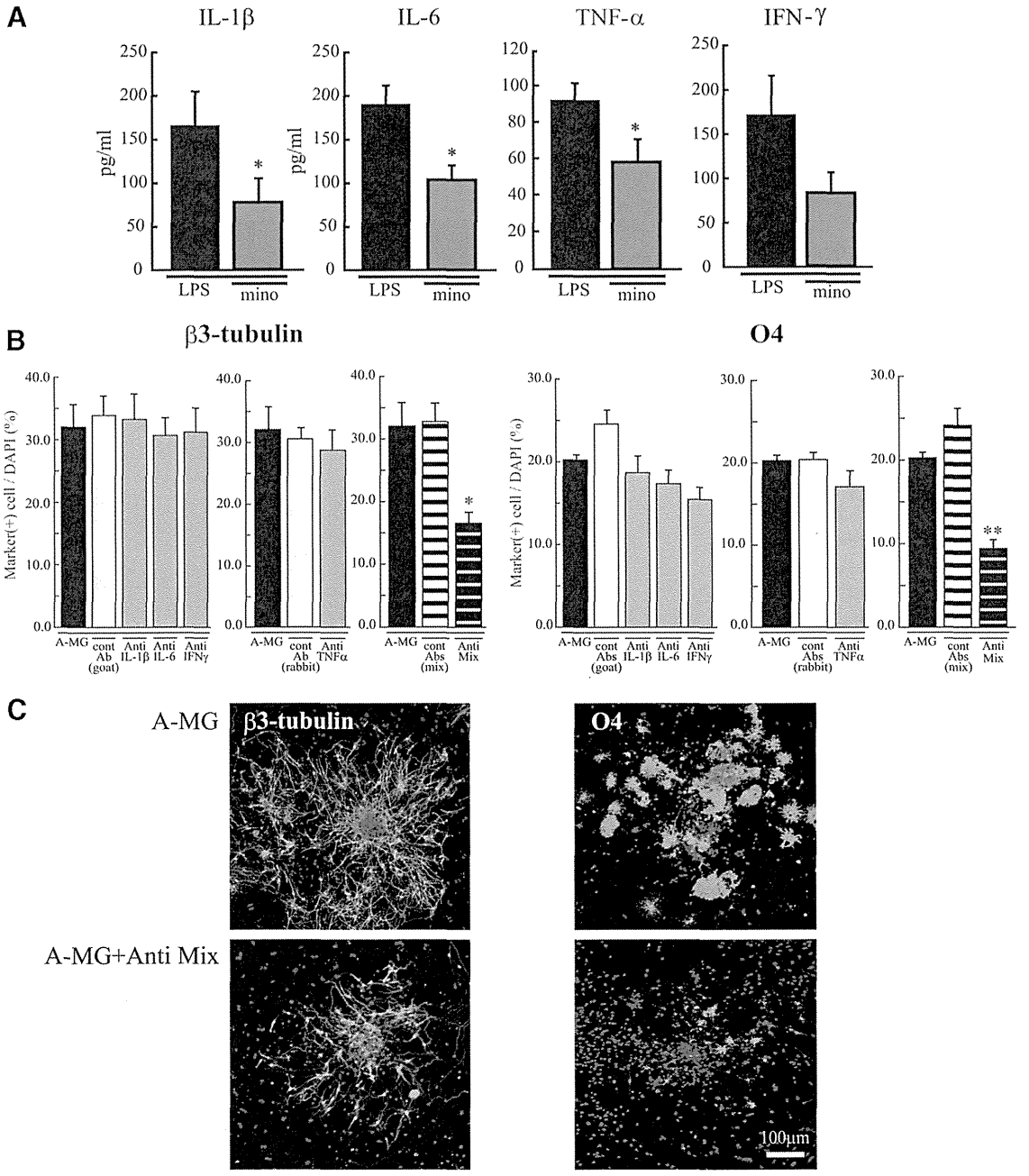

Figure 7. The *in vitro* enhancement of neurogenesis and oligodendrogenesis by activated microglia was suppressed by the mixture of function-blocking antibodies (anti-IL-1β, anti-IL-6, anti-TNF-α, and anti-IFN-γ). ***A***, The release of IL-1β, IL-6, TNF-α, or IFN-γ from activated microglia was suppressed by minocycline. Cultured microglia were activated by LPS (10 ng/ml, 30 min) in the absence and presence of minocycline (10 μM). The concentration of each cytokine in the supernatant was measured by ELISA 24 h after. *$p < 0.05$ (Student's *t* test). Data are mean ± SEM. ***B***, Effects of function-blocking antibodies to IL-1β, IL-6, TNF-α, and IFN-γ on enhanced neurogenesis and oligodendrogenesis by the activated microglia. The neurospheres were differentiated in the absence or presence of functional blocking antibodies (goat anti-rat IL-1β antibody, goat anti-rat IL-6 antibody, TNF-α antibody, or goat anti-mouse/rat IFN-γ antibody) (1 μg/ml for each) and a mixture of all of these antibodies. After a differentiation period suitable for neurons (7 d) or oligodendrocytes (11 d), neurospheres were stained for β3-tubulin (green), O4 (green), and TOTO3 (cyan). The data of single function blocking antibodies were compared with the controls, which include the same concentration of isotype-matched control IgGs (1 μg/ml for each). The data of the mixture of function blocking antibodies were compared with the controls, which include the same concentrations of isotype-matched control IgGs (i.e., 3 μg/ml of normal goat IgG control and 1 μg/ml of rabbit IgG control). *$p < 0.05$. **$p < 0.01$, versus isotype-matched control IgG group (Tukey's test by ANOVA). Data are mean ± SEM. ***C***, Representative immunostained images of neurospheres cocultured with activated microglia in the absence or presence of the mixture of the function-blocking antibodies. We confirmed the same results in three independent experiments.

for β3-tubulin or O4. We further confirmed these results using a differentiation assay with cells dissociated from neurospheres (Fig. 6*C*,*D*). With this protocol, the morphology of each cell could be discriminated more clearly. Consistent with the results described above, an increase in the numbers of cells positive for β3-tubulin and O4 was induced by activated microglia (Fig. 6*C*,*D*). Of note, PDGFRα^+ cells were decreased by activated microglia, whereas O4$^+$ cells were increased by activated microglia. Minocycline suppressed both of these effects, suggesting that activated microglia affect the later stage of oligodendrogenesis, thereby reducing the size of PDGFα^+ progenitor pool. In this experiment, we also checked the effects of minocycline alone (10 μM) on neurogenesis and oligodendrogenesis (Fig. 6*C*, "mino-cont" in each graph). Minocycline did not affect the numbers of

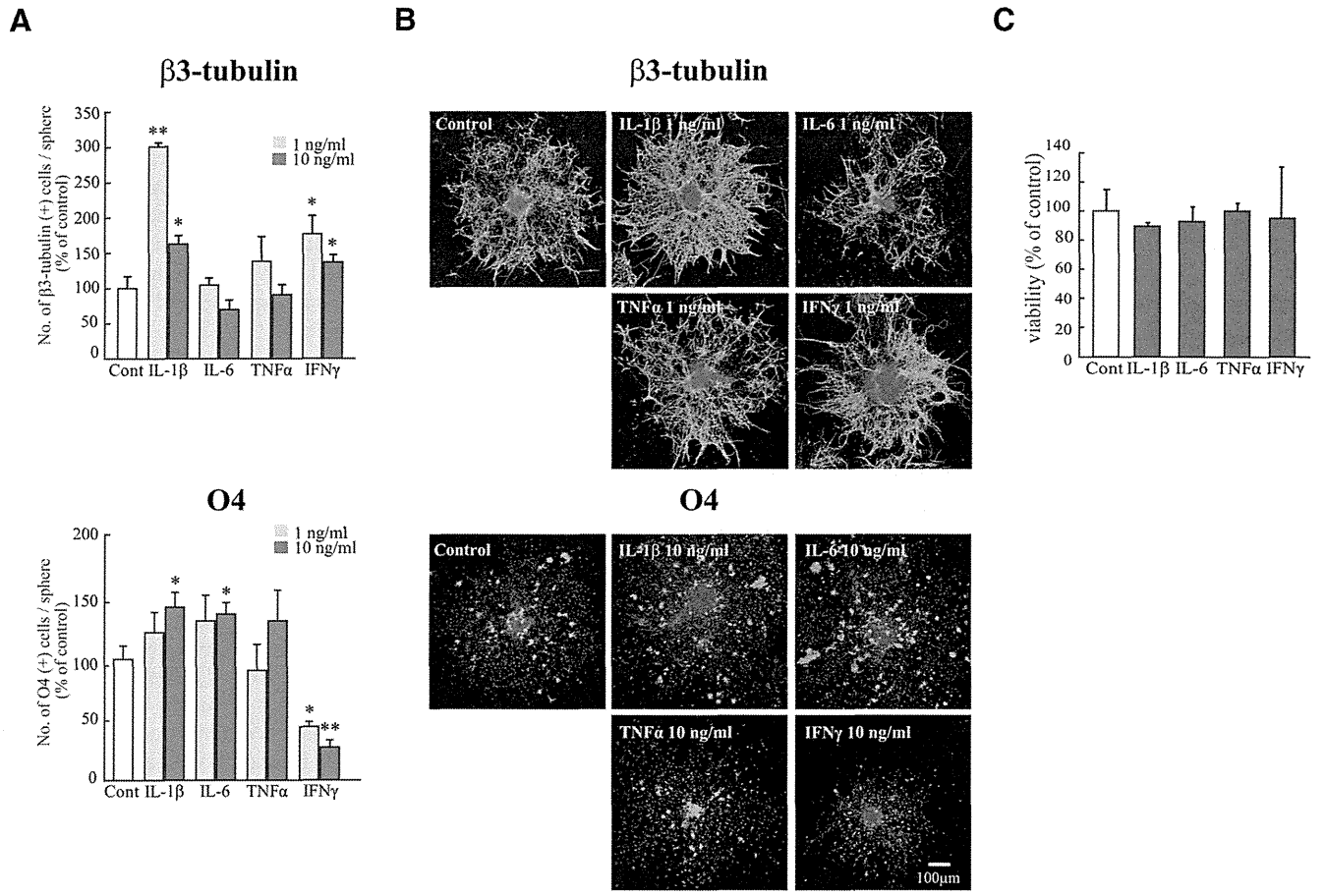

Figure 8. The effect of each cytokine on neurogenesis and oligodendrogenesis. Neurospheres were incubated for differentiation period suitable for neurons (7 d) or oligodendrocytes (11 d) in the presence of each single cytokine (rIL-1β, rIL-6, rTNF-α, or rIFN-γ) at 1–10 ng/ml. Neurospheres were stained for β3-tubulin (green), O4 (green), followed by TOTO3 (cyan). ***A***, Quantification of the effects of cytokines on neurogenesis and oligodendrogenesis. IL-1β and IFN-γ significantly enhanced neurogenesis at 1 ng/ml. IL-1β and IL-6 enhanced oligodendrogenesis at 10 ng/ml. $^*p < 0.05$ versus control (Tukey's test by ANOVA). $^{**}p < 0.01$ versus control (Tukey's test by ANOVA). $n = 8$ neurospheres/group. Data are mean ± SEM. ***B***, Representative images of neurospheres immunostained for β3-tubulin and O4 after differentiation in the presence of the cytokine. ***C***, The effect of each cytokine (10 ng/ml) on cell viability. They did not affect cell viability at 10 ng/ml. The same results were obtained in two independent experiments.

cells positive for β3-tubulin, O4, PDGFRα, or GFAP, indicating that minocycline itself had little direct effects on neurogenesis and oligodendrogenesis. Together, these results demonstrated that we could reproduce the *in vivo* data in an *in vitro* coculture experiment. We further confirmed that activated microglia enhanced neurogenesis and oligodendrogenesis, and minocycline specifically suppressed the effects of microglia. We therefore examined the effects of minocycline on the release of IL-1β, IL-6, TNF-α, and IFN-γ from activated microglia *in vitro*. In the presence of minocycline, the release of all of these cytokines was significantly suppressed (Fig. 7*A*), consistent with *in vivo* data (Fig. 5*C*). To examine the extent of the contribution of each cytokine to the enhancement of neurogenesis and oligodendrogenesis, we applied function-blocking antibodies to IL-1β, IL-6, TNF-α, and IFN-γ (1 μg/ml) to cocultures of activated microglia and neurospheres (Fig. 7*B*). The same concentration of isotype-matched control IgG (both of goat and rabbit) (1 μg/ml) did not have any effects on either neurogenesis or oligodendrogenesis. Unexpectedly, any single function-blocking antibody to IL-1β, IL-6, TNF-α, or IFN-γ did not change the effects of activated microglia on neurogenesis and oligodendrogenesis (Fig. 7*B*). We then tried a mixture of all of these function-blocking antibodies (goat anti-rat IL-1β antibody, goat anti-rat IL-6 antibody, TNF-α antibody, and goat anti-mouse/rat IFN-γ antibody, 1 μg/ml for each). When compared with the control which included the same concentrations of isotype-matched control IgGs (i.e., 3 μg/ml of normal goat IgG control and 1 μg/ml of rabbit IgG control), the effects of activated microglia were significantly suppressed by a mixture of all of these function-blocking antibodies (Fig. 7*B*, Anti Mix in the right graphs in β3-tubulin and O4, respectively). The representative images of the expression of β3-tubulin (left) or O4 (right) in neurospheres cocultured with activated microglia in the presence of the mixture of function-blocking antibodies are shown in Figure 7*C*. We also examined the direct effects of each single cytokine on neurogenesis and oligodendrogenesis separately (Fig. 8). IL-1β and IFN-γ enhanced neurogenesis at 1 ng/ml, although the effects became weaker at 10 ng/ml (Fig. 8*A*). IL-1β and IL-6 enhanced oligodendrogenesis at 10 ng/ml (Fig. 8*A*). IFN-γ suppressed oligodendrogenesis. These results suggest that IL-1β and IFN-γ are important for neurogenesis, whereas IL-1β and IL-6 are important for oligodendrogenesis, and the combinations and concentrations optimal for neurogenesis and oligodendrogenesis are different. Representative data of the neurospheres treated with the cytokines are shown in Figure 8*B*. We confirmed that each single cytokine did not affect cell viability at 10 ng/ml in our experimental protocol (Fig. 8*C*). These *in vitro* data indicate that activated microglia regulate neurogenesis and oligodendrogenesis through released cytokines, and the cyto-

kines produce their effects in a synergistic manner. It also appears that the combinations and concentrations optimal for neurogenesis and oligodendrogenesis are different.

Discussion

In the postnatal mammalian brain, neural stem cells (NSCs) are mainly localized in two areas: the forebrain SVZ (Doetsch and Scharff, 2001) and the subgranular zone of the dentate gyrus (Zerlin et al., 2004) of the hippocampus (Gould et al., 1999; Lie et al., 2004). The microenvironments that are permissive for neurogenesis and gliogenesis are composed of a variety of cell types, such as stem cells, progenitor cells, astrocyte cells, and microglial cells. Increasing evidence indicates the importance of the surrounding glial cells in neurogenesis (Doetsch et al., 1999; Temple, 2001). Goings et al. (2006) have shown that microglia in the adult SVZ are semiactivated, but microglial contribution to neurogenesis is complex. So far, the role of microglia in neurogenesis has been examined mainly in pathological conditions (Ekdahl et al., 2003; Monje et al., 2003). Activated microglia in inflammatory settings, such as intraperitoneal administration of LPS, inhibited neurogenesis (Ekdahl et al., 2003; Monje et al., 2003; Cacci et al., 2008). However, a growing number of studies have suggested that activated microglia are beneficial for neurogenesis (Aarum et al., 2003; Butovsky et al., 2005, 2006a; Walton et al., 2006; Ziv et al., 2006; Hanisch and Kettenmann, 2007; Ekdahl et al., 2009; Bachstetter et al., 2011; Ekdahl, 2012; Vukovic et al., 2012), even in pathological conditions, such as an animal model of multiple sclerosis (Butovsky et al., 2006b), ischemia (Thored et al., 2009; Deierborg et al., 2010), and epilepsy (Bonde et al., 2006). Such variability concerning the effects of microglia on neurogenesis may reflect the different polarization of microglia and/or the precise status of NSCs/neuronal progenitor cells (NPCs) (Cacci et al., 2008; Li et al., 2010; Ekdahl, 2012; Ortega et al., 2013), and crosstalk between them (Mosher et al., 2012).

Concerning the origin of microglia, various data have been reported. *In vivo* lineage tracing studies have established that microglia differentiate from primitive myeloid progenitors that arise before embryonic day 8 and are identified in the CNS parenchyma even before definitive hematopoiesis (Ginhoux et al., 2010), although it has been shown that microglia migrate from lateral ventricle into brain via SVZ in the postnatal brain (Mohri et al., 2003). Microglia in the embryonic SVZ limit the production of cortical neurons by phagocytosing neural precursor cells (Cunningham et al., 2013). Even in the adult brain, microglia appear densely populated in neurogenic niches, such as the SVZ (Mosher et al., 2012), and appear more activated in the adult SVZ than in non-neurogenic zones (Goings et al., 2006). Although these data strongly suggest that microglia play important roles in CNS development and an increasing number of studies have elucidated various roles of microglia during developmental periods (Wu et al., 1993; Pont-Lezica et al., 2011; Tremblay et al., 2011), the detailed dynamics of microglia in the SVZ from early postnatal stages to a young adult stage remain to be elucidated. Furthermore, few studies have examined the role of microglia in normal developmental processes during this period. In this study, we found that activated microglia first accumulated in the SVZ and then dispersed to white matter, where they became more ramified. In addition, the number of activated microglia was largest in the medial SVZ throughout the studied period (P30). We here elucidated that activated microglia in the early postnatal SVZ enhance neurogenesis and oligodendrogenesis through the mechanisms described below. Our present data and the previous reports concerning developmental changes in the distribution suggest that the developmental roles of microglia in the SVZ are not transient but more general throughout life.

Using a combination of *in vivo* and *in vitro* approaches, we demonstrated that these activated microglia in the early postnatal SVZ enhanced neurogenesis and oligodendrogenesis through releasing cytokines. Butovsky et al. (2006a) reported that the beneficial effects of microglia on adult neurogenesis/oligodendrogenesis was achieved by IGF-1 after IL-4 and IFN-γ release from activated microglia. In our study, although the activated microglia in the early postnatal SVZ did produce IGF-1, the effects of activated microglia on neurogenesis and oligodendrogenesis observed here were independent of IGF-1. We clarified that the SVZ microglia facilitate neurogenesis and oligodendrogenesis via production of cytokines. Interestingly, in *in vitro* coculture experiments, the enhancement of neurogenesis and oligodendrogenesis was suppressed by a mixture of function-blocking antibodies (anti-IL-1β, anti-IL-6, anti-TNF-α, anti-IFN-γ), but not by a single function-blocking antibody. These results suggest that microglial cytokines enhance neurogenesis and oligodendrogenesis in combinations. In support of this, among the cytokines we examined, only IL-1β and IFN-γ enhanced neurogenesis, whereas only IL-1β and IL-6 showed potentials of enhancing oligodendrogenesis. Previous reports have shown that NPCs express IL-1β, IL-1RI and IL-1RII, and IL-1β regulates the proliferation and differentiation of NPCs (Wang et al., 2007). It has been shown that IL-1β promotes proliferation and differentiation of oligodendrocyte progenitor cells (Vela et al., 2002). Furthermore, IL-6 and IL-6R are reported to promote neurogenesis and gliogenesis (Islam et al., 2009; Oh et al., 2010). Li et al. (2010) showed that IFN-γ stimulated neurosphere formation from embryonic brain, but the effects of IFN-γ are modified in the presence of microglia, supporting the complementary interactions between cytokines.

These proinflammatory cytokines had been thought to cause suppression of neurogenesis in pathological conditions, such as chronic LPS stimulation (Monje et al., 2003), allergic encephalomyelitis (Ben-Hur et al., 2003), and status epilepticus (Iosif et al., 2006; Koo and Duman, 2008). However, recent reports have shown that that the different polarizations of microglia are induced by different application protocols of LPS (Cacci et al., 2008), suggesting that the combination and the concentration of cytokines released by microglia change depending on the ambient conditions. Indeed, some previous reports suggest that each cytokine reveals different effects at different concentrations (Bernardino et al., 2008; Cacci et al., 2008; Das and Basu, 2008; Russo et al., 2011). Bernardino et al. (2008) have shown that TNF-α results in proliferation of neural stem cells at 1 ng/ml but caused apoptosis at 10–100 ng/ml. Microglia in the developmental brains may sense the change of environment and release a certain combination of cytokines at suitable concentrations for neurogenesis and oligodendrogenesis, whereas overactivation of microglia in pathological inflammation or nerve injury induces massive proinflammatory cytokine production, resulting in the suppression of neurogenesis. Nakanishi et al. (2007) showed that IL-6 promoted astrocytogenesis from the SVZ neurospheres. In our study, however, although activated microglia release IL-6, the effects on astrocytogenesis were not observed either *in vivo* or *in vitro*. This might be because of different medium compositions (i.e., growth factors) used for differentiation of neurosphere. Compared with the other cytokines, only IFN-γ suppressed oligodendrogenesis, suggesting that a proper concentration range of IFN-γ to enhance oligodendrogenesis might be narrower than the other cytokines.

Of interest, our results suggest that activated microglia significantly increased $O4^+$ cells while decreasing $PDGFR\alpha^+$ cells. These results suggest that activated microglia enhance oligodendrogenesis at later stages of oligodendrocyte differentiation. Recently, Miron et al. (2013) showed that a switch from M1 to M2 occurred in microglia during remyelination, and oligodendrocyte differentiation was enhanced by M2 cell releasing factors. A comprehensive analysis about the released factors from microglia, including cytokines, and the precise identification of the cell population (NSCs and/or NPCs) that are responsive to these factors will be necessary to understand fully the mechanisms underlying the effects of microglia on neurogenesis and gliogenesis.

In conclusion, we have found a population of activated microglia accumulating in the early postnatal SVZ that facilitate neurogenesis and oligodendrogenesis. A synergism among cytokines was important for the effects. To our knowledge, this is the first report to show that microglia regulate cell differentiation via releasing cytokines in early postnatal brain development.

References

Aarum J, Sandberg K, Haeberlein SL, Persson MA (2003) Migration and differentiation of neural precursor cells can be directed by microglia. Proc Natl Acad Sci U S A 100:15983–15988. CrossRef Medline

Bachstetter AD, Morganti JM, Jernberg J, Schlunk A, Mitchell SH, Brewster KW, Hudson CE, Cole MJ, Harrison JK, Bickford PC, Gemma C (2011) Fractalkine and CX 3 CR1 regulate hippocampal neurogenesis in adult and aged rats. Neurobiol Aging 32:2030–2044. CrossRef Medline

Ben-Hur T, Ben-Menachem O, Furer V, Einstein O, Mizrachi-Kol R, Grigoriadis N (2003) Effects of proinflammatory cytokines on the growth, fate, and motility of multipotential neural precursor cells. Mol Cell Neurosci 24:623–631. CrossRef Medline

Bernardino L, Agasse F, Silva B, Ferreira R, Grade S, Malva JO (2008) Tumor necrosis factor-alpha modulates survival, proliferation, and neuronal differentiation in neonatal subventricular zone cell cultures. Stem Cells 26:2361–2371. CrossRef Medline

Bonde S, Ekdahl CT, Lindvall O (2006) Long-term neuronal replacement in adult rat hippocampus after status epilepticus despite chronic inflammation. Eur J Neurosci 23:965–974. CrossRef Medline

Butovsky O, Talpalar AE, Ben-Yaakov K, Schwartz M (2005) Activation of microglia by aggregated beta-amyloid or lipopolysaccharide impairs MHC-II expression and renders them cytotoxic whereas IFN-gamma and IL-4 render them protective. Mol Cell Neurosci 29:381–393. CrossRef Medline

Butovsky O, Ziv Y, Schwartz A, Landa G, Talpalar AE, Pluchino S, Martino G, Schwartz M (2006a) Microglia activated by IL-4 or IFN-gamma differentially induce neurogenesis and oligodendrogenesis from adult stem/progenitor cells. Mol Cell Neurosci 31:149–160. CrossRef Medline

Butovsky O, Landa G, Kunis G, Ziv Y, Avidan H, Greenberg N, Schwartz A, Smirnov I, Pollack A, Jung S, Schwartz M (2006b) Induction and blockage of oligodendrogenesis by differently activated microglia in an animal model of multiple sclerosis. J Clin Invest 116:905–915. CrossRef Medline

Cacci E, Ajmone-Cat MA, Anelli T, Biagioni S, Minghetti L (2008) In vitro neuronal and glial differentiation from embryonic or adult neural precursor cells are differently affected by chronic or acute activation of microglia. Glia 56:412–425. CrossRef Medline

Camacho-Arroyo I, López-Griego L, Morales-Montor J (2009) The role of cytokines in the regulation of neurotransmission. Neuroimmunomodulation 16:1–12. CrossRef Medline

Cunningham CL, Martínez-Cerdeño V, Noctor SC (2013) Microglia regulate the number of neural precursor cells in the developing cerebral cortex. J Neurosci 33:4216–4233. CrossRef Medline

Das S, Basu A (2008) Inflammation: a new candidate in modulating adult neurogenesis. J Neurosci Res 86:1199–1208. CrossRef Medline

Deierborg T, Roybon L, Inacio AR, Pesic J, Brundin P (2010) Brain injury activates microglia that induce neural stem cell proliferation ex vivo and promote differentiation of neurosphere-derived cells into neurons and oligodendrocytes. Neuroscience 171:1386–1396. CrossRef Medline

Doetsch F, Scharff C (2001) Challenges for brain repair: insights from adult neurogenesis in birds and mammals. Brain Behav Evol 58:306–322. CrossRef Medline

Doetsch F, García-Verdugo JM, Alvarez-Buylla A (1999) Regeneration of a germinal layer in the adult mammalian brain. Proc Natl Acad Sci U S A 96:11619–11624. CrossRef Medline

Ekdahl CT (2012) Microglial activation- tuning and pruning adult neurogenesis. Front Pharmacol 3:41. CrossRef Medline

Ekdahl CT, Claasen JH, Bonde S, Kokaia Z, Lindvall O (2003) Inflammation is detrimental for neurogenesis in adult brain. Proc Natl Acad Sci U S A 100:13632–13637. CrossRef Medline

Ekdahl CT, Kokaia Z, Lindvall O (2009) Brain inflammation and adult neurogenesis: the dual role of microglia. Neuroscience 158:1021–1029. CrossRef Medline

Ginhoux F, Greter M, Leboeuf M, Nandi S, See P, Gokhan S, Mehler MF, Conway SJ, Ng LG, Stanley ER, Samokhvalov IM, Merad M (2010) Fate mapping analysis reveals that adult microglia derive from primitive macrophages. Science 330:841–845. CrossRef Medline

Goings GE, Kozlowski DA, Szele FG (2006) Differential activation of microglia in neurogenic versus non-neurogenic regions of the forebrain. Glia 54:329–342. CrossRef Medline

Gould E, Reeves AJ, Graziano MS, Gross CG (1999) Neurogenesis in the neocortex of adult primates. Science 286:548–552. CrossRef Medline

Hamanoue M, Matsuzaki Y, Sato K, Okano HJ, Shibata S, Sato I, Suzuki S, Ogawara M, Takamatsu K, Okano H (2009) Cell surface N-glycans mediated isolation of mouse neural stem cells. J Neurochem 110:1575–1584. CrossRef Medline

Hanisch UK, Kettenmann H (2007) Microglia: active sensor and versatile effector cells in the normal and pathologic brain. Nat Neurosci 10:1387–1394. CrossRef Medline

Hirasawa T, Ohsawa K, Imai Y, Ondo Y, Akazawa C, Uchino S, Kohsaka S (2005) Visualization of microglia in living tissues using Iba1-EGFP transgenic mice. J Neurosci Res 81:357–362. CrossRef Medline

Ignácio AR, Müller YM, Carvalho MS, Nazari EM (2005) Distribution of microglial cells in the cerebral hemispheres of embryonic and neonatal chicks. Braz J Med Biol Res 38:1615–1621. Medline

Inoue K (2008) Purinergic systems in microglia. Cell Mol Life Sci 65:3074–3080. CrossRef Medline

Iosif RE, Ekdahl CT, Ahlenius H, Pronk CJ, Bonde S, Kokaia Z, Jacobsen SE, Lindvall O (2006) Tumor necrosis factor receptor 1 is a negative regulator of progenitor proliferation in adult hippocampal neurogenesis. J Neurosci 26:9703–9712. CrossRef Medline

Islam O, Gong X, Rose-John S, Heese K (2009) Interleukin-6 and neural stem cells: more than gliogenesis. Mol Biol Cell 20:188–199. CrossRef Medline

Kettenmann H, Hanisch UK, Noda M, Verkhratsky A (2011) Physiology of microglia. Physiol Rev 91:461–553. CrossRef Medline

Koo JW, Duman RS (2008) IL-1beta is an essential mediator of the antineurogenic and anhedonic effects of stress. Proc Natl Acad Sci U S A 105:751–756. CrossRef Medline

Li L, Walker TL, Zhang Y, Mackay EW, Bartlett PF (2010) Endogenous interferon gamma directly regulates neural precursors in the non-inflammatory brain. J Neurosci 30:9038–9050. CrossRef Medline

Lie DC, Song H, Colamarino SA, Ming GL, Gage FH (2004) Neurogenesis in the adult brain: new strategies for central nervous system diseases. Annu Rev Pharmacol Toxicol 44:399–421. CrossRef Medline

Marshall GP 2nd, Demir M, Steindler DA, Laywell ED (2008) Subventricular zone microglia possess a unique capacity for massive in vitro expansion. Glia 56:1799–1808. CrossRef Medline

Miller RJ, Jung H, Bhangoo SK, White FA (2009) Cytokine and chemokine regulation of sensory neuron function. Handb Exp Pharmacol 194:417–449. CrossRef Medline

Miron VE, Boyd A, Zhao JW, Yuen TJ, Ruckh JM, Shadrach JL, van Wijngaarden P, Wagers AJ, Williams A, Franklin RJ, ffrench-Constant C (2013) M2 microglia and macrophages drive oligodendrocyte differentiation during CNS remyelination. Nat Neurosci 16:1211–1218. CrossRef Medline

Mohri I, Eguchi N, Suzuki K, Urade Y, Taniike M (2003) Hematopoietic prostaglandin D synthase is expressed in microglia in the developing postnatal mouse brain. Glia 42:263–274. CrossRef Medline

Monje ML, Toda H, Palmer TD (2003) Inflammatory blockade restores adult hippocampal neurogenesis. Science 302:1760–1765. CrossRef Medline

Monji A, Kato T, Kanba S (2009) Cytokines and schizophrenia: microglia

hypothesis of schizophrenia. Psychiatry Clin Neurosci 63:257–265. CrossRef Medline

Mosher KI, Andres RH, Fukuhara T, Bieri G, Hasegawa-Moriyama M, He Y, Guzman R, Wyss-Coray T (2012) Neural progenitor cells regulate microglia functions and activity. Nat Neurosci 15:1485–1487. CrossRef Medline

Nakajima K, Kohsaka S (2001) Microglia: activation and their significance in the central nervous system. J Biochem 130:169–175. CrossRef Medline

Nakajima K, Tsuzaki N, Shimojo M, Hamanoue M, Kohsaka S (1992) Microglia isolated from rat brain secrete a urokinase-type plasminogen activator. Brain Res 577:285–292. CrossRef Medline

Nakanishi M, Niidome T, Matsuda S, Akaike A, Kihara T, Sugimoto H (2007) Microglia-derived interleukin-6 and leukaemia inhibitory factor promote astrocytic differentiation of neural stem/progenitor cells. Eur J Neurosci 25:649–658. CrossRef Medline

Nishiyama A, Komitova M, Suzuki R, Zhu X (2009) Polydendrocytes (NG2 cells): multifunctional cells with lineage plasticity. Nat Rev Neurosci 10: 9–22. CrossRef Medline

Oh J, McCloskey MA, Blong CC, Bendickson L, Nilsen-Hamilton M, Sakaguchi DS (2010) Astrocyte-derived interleukin-6 promotes specific neuronal differentiation of neural progenitor cells from adult hippocampus. J Neurosci Res 88:2798–2809. CrossRef Medline

Ortega F, Gascón S, Masserdotti G, Deshpande A, Simon C, Fischer J, Dimou L, Chichung Lie D, Schroeder T, Berninger B (2013) Oligodendrogliogenic and neurogenic adult subependymal zone neural stem cells constitute distinct lineages and exhibit differential responsiveness to Wnt signalling. Nat Cell Biol 15:602–613. CrossRef Medline

Pont-Lezica L, Béchade C, Belarif-Cantaut Y, Pascual O, Bessis A (2011) Physiological roles of microglia during development. J Neurochem 119: 901–908. CrossRef Medline

Reynolds BA, Tetzlaff W, Weiss S (1992) A multipotent EGF-responsive striatal embryonic progenitor cell produces neurons and astrocytes. J Neurosci 12:4565–4574. Medline

Russo I, Barlati S, Bosetti F (2011) Effects of neuroinflammation on the regenerative capacity of brain stem cells. J Neurochem 116:947–956. CrossRef Medline

Schäfers M, Sorkin L (2008) Effect of cytokines on neuronal excitability. Neurosci Lett 437:188–193. CrossRef Medline

Spedding M, Gressens P (2008) Neurotrophins and cytokines in neuronal plasticity. Novartis Found Symp 289:222–233; discussion 233–240. Medline

Spooren A, Kolmus K, Laureys G, Clinckers R, De Keyser J, Haegeman G, Gerlo S (2011) Interleukin-6, a mental cytokine. Brain Res Rev 67:157–183. CrossRef Medline

Suzuki SO, Goldman JE (2003) Multiple cell populations in the early postnatal subventricular zone take distinct migratory pathways: a dynamic study of glial and neuronal progenitor migration. J Neurosci 23:4240–4250. Medline

Temple S (2001) The development of neural stem cells. Nature 414:112–117. CrossRef Medline

Thored P, Heldmann U, Gomes-Leal W, Gisler R, Darsalia V, Taneera J, Nygren JM, Jacobsen SE, Ekdahl CT, Kokaia Z, Lindvall O (2009) Long-term accumulation of microglia with proneurogenic phenotype concomitant with persistent neurogenesis in adult subventricular zone after stroke. Glia 57:835–849. CrossRef Medline

Tikka T, Fiebich BL, Goldsteins G, Keinanen R, Koistinaho J (2001) Minocycline, a tetracycline derivative, is neuroprotective against excitotoxicity by inhibiting activation and proliferation of microglia. J Neurosci 21: 2580–2588. Medline

Tremblay MÈ, Stevens B, Sierra A, Wake H, Bessis A, Nimmerjahn A (2011) The role of microglia in the healthy brain. J Neurosci 31:16064–16069. CrossRef Medline

Vela JM, Molina-Holgado E, Arévalo-Martín A, Almazán G, Guaza C (2002) Interleukin-1 regulates proliferation and differentiation of oligodendrocyte progenitor cells. Mol Cell Neurosci 20:489–502. CrossRef Medline

Vukovic J, Colditz MJ, Blackmore DG, Ruitenberg MJ, Bartlett PF (2012) Microglia modulate hippocampal neural precursor activity in response to exercise and aging. J Neurosci 32:6435–6443. CrossRef Medline

Wagner JP, Black IB, DiCicco-Bloom E (1999) Stimulation of neonatal and adult brain neurogenesis by subcutaneous injection of basic fibroblast growth factor. J Neurosci 19:6006–6016. Medline

Walton NM, Sutter BM, Laywell ED, Levkoff LH, Kearns SM, Marshall GP 2nd, Scheffler B, Steindler DA (2006) Microglia instruct subventricular zone neurogenesis. Glia 54:815–825. CrossRef Medline

Wang X, Fu S, Wang Y, Yu P, Hu J, Gu W, Xu XM, Lu P (2007) Interleukin-1beta mediates proliferation and differentiation of multipotent neural precursor cells through the activation of SAPK/JNK pathway. Mol Cell Neurosci 36:343–354. CrossRef Medline

Wu CH, Wen CY, Shieh JY, Ling EA (1993) A quantitative study of the differentiation of microglial cells in the developing cerebral cortex in rats. J Anat 182:403–413. Medline

Xu J, Ling EA (1994) Studies of the distribution and functional roles of transitory amoeboid microglial cells in developing rat brain using exogenous horseradish peroxidase as a marker. J Hirnforsch 35:103–111. Medline

Zerlin M, Milosevic A, Goldman JE (2004) Glial progenitors of the neonatal subventricular zone differentiate asynchronously, leading to spatial dispersion of glial clones and to the persistence of immature glia in the adult mammalian CNS. Dev Biol 270:200–213. CrossRef Medline

Zhao C, Ling Z, Newman MB, Bhatia A, Carvey PM (2007) TNF-alpha knockout and minocycline treatment attenuates blood–brain barrier leakage in MPTP-treated mice. Neurobiol Dis 26:36–46. CrossRef Medline

Ziv Y, Ron N, Butovsky O, Landa G, Sudai E, Greenberg N, Cohen H, Kipnis J, Schwartz M (2006) Immune cells contribute to the maintenance of neurogenesis and spatial learning abilities in adulthood. Nat Neurosci 9:268–275. CrossRef Medline

Bioconjugate Chemistry

Communication

pubs.acs.org/bc

Development of Cell-Penetrating R7 Fragment-Conjugated Helical Peptides as Inhibitors of Estrogen Receptor-Mediated Transcription

Takaya Nagakubo,[†,‡] Yosuke Demizu,[*,†] Yasunari Kanda,[†] Takashi Misawa,[†] Takuji Shoda,[†] Keiichiro Okuhira,[†] Yuko Sekino,[†] Mikihiko Naito,[†] and Masaaki Kurihara[*,†,‡]

[†]National Institute of Health Sciences, Tokyo 158-8501, Japan

[‡]Graduate School of Bioscience and Biotechnology, Tokyo Institute of Technology, Yokohama 226-8501, Japan

S *Supporting Information*

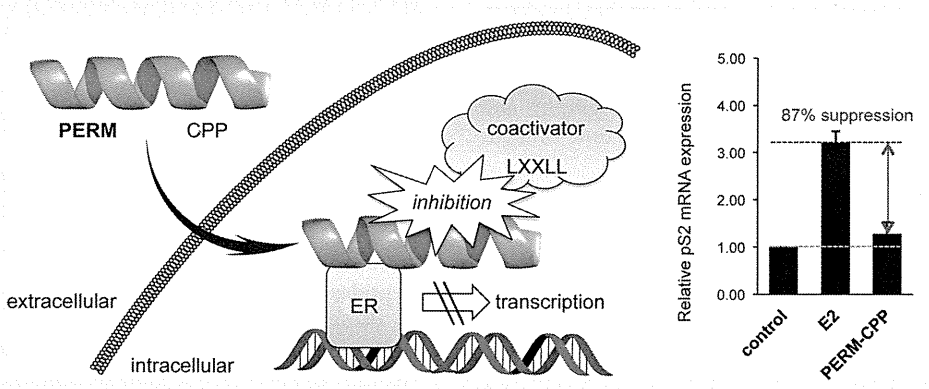

ABSTRACT: The heptaarginine (R7)-conjugated peptide **5** was designed and synthesized as an inhibitor of ER-coactivator interactions and ER-mediated transcription at the cellular level. The R7-conjugated peptide **5** was able to enter ER-positive T47D cells efficiently, and treatment with 3 μM of **5** downregulated the mRNA expression of pS2 (an ER-mediated gene) by 87%.

INTRODUCTION

Breast cancer is the most common cancer in women, and its incidence is increasing from year to year. The estrogen receptor (ER), which is a ligand-inducible transcription factor and a member of the nuclear receptor superfamily, is often overexpressed in the tissues of breast cancer patients and promotes the estrogen-dependent proliferation of cancer cells.[1−3] Several ERα antagonistic drugs, such as tamoxifen and nonsteroidal selective ER modulators, have been developed as treatments for breast cancer.[4−8] Among those antagonists, tamoxifen acts via the competitive inhibition of 17β-estradiol (E2) and is the most widely used drug for treating breast cancer.[9,10] However, tamoxifen has agonistic effects on ERα in uterine cancer cells and increases the risk of endometrial cancer.[11,12] In addition, it activates the protein kinase B (Akt) signaling pathway by binding to a particular ER variant, resulting in the inhibition of apoptosis in cancer cells.[13,14] Therefore, novel drug candidates with different mechanisms of action have long been desired. ER-mediated gene activation is induced by the binding of E2 to the ER ligand-binding domain and the subsequent binding of the consensus LXXLL helical motif[15] (L: leucine, X: any amino acid residue) of the coactivator with the ER surface.[16,17] Helical peptides containing the above-mentioned consensus sequence have been demonstrated to inhibit ER-coactivator interactions, and they are also considered to be drug candidates for reducing ER-mediated transactivation. Various helical peptides have been reported as inhibitors of ER-coactivator interactions.[18−22] The peptidomimetic estrogen receptor modulators (PERMs), specifically, PERM-1 and PERM-3 [with two mutation: Lys(1) → Arg(1) and Leu(7) → Npg(7)] reported by Burris et al. exhibited particularly potent inhibitory activity against ER-coactivator interactions.[19,20] However, only a few peptide-based ER-transcription inhibitors that exhibit potent activity at the cellular level have been reported[23,24] because of the low cell permeability of such peptides. Thus, we assumed that the conjugation of PERM with cell-penetrating peptides such as oligoarginines and their derivatives[25,26] might solve the problems surrounding the development of novel peptide-based transcriptional inhibitors (Figure 1). In this communication, we describe the synthesis of heptaarginine (R7)-conjugated PERM as inhibitors of ER-signaling at the cellular level (Table 1). Specifically, we synthesized R7-conjugated helical peptides and evaluated their cellular uptake, ability to inhibit transcription in ER-positive T47D cells, ability to inhibit ER-coactivator interactions, and their preferred secondary structures (by assessing their CD spectra).

RESULTS AND DISCUSSION

Synthesis of Peptides. The N-terminal-free peptides **1**−**7** and their N-terminal fluorescein (FAM) labeled peptides were

Received: October 17, 2014
Revised: November 5, 2014
Published: November 6, 2014

dx.doi.org/10.1021/bc500480e | *Bioconjugate Chem.* 2014, 25, 1921−1924

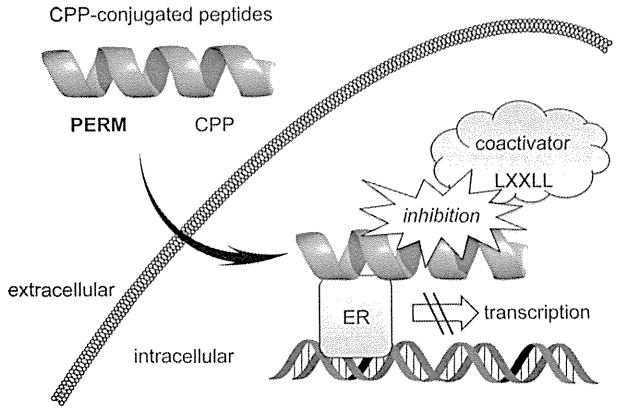

Figure 1. Illustration of the mechanism by which the CPP-conjugated peptides inhibited ER-coactivator interactions at the cellular level.

synthesized using microwave-assisted Fmoc-based solid phase methods, respectively. All of the peptides were purified by reversed-phase high performance liquid chromatography and were characterized using electrospray ionization time-of-flight mass spectrometry (Supporting Information).

Biological Evaluations. First of all, we evaluated the cellular uptake of fluorescein-labeled peptides (green; 1 μM) into ER-positive T47D cells (incubated for 3 h) using confocal laser scanning microscopy (CLSM, Supporting Information) as shown in Figure 2. The R7-unconjugated peptide **FAM-2** (an N-terminal fluorescein-labeled version of peptide **2**) was completely unable to enter the ER-positive T47D cells, whereas the R7-conjugated peptide **FAM-5** passed through the cell membrane efficiently and was distributed in the cytoplasm and nucleus. This difference in the cell-penetrating abilities of the molecules was solely due to the presence/absence of R7 conjugation. The R7-conjugated peptide **FAM-4** also exhibited cell permeability (Supporting Information).

Then, we evaluated the ability of the R7-conjugated peptides to inhibit ER-mediated transcription. Transcriptional analysis of an ER target gene (pS2) was carried out using T47D cells that had been incubated with one of the peptides (3 μM) in the absence or presence of 10 nM E2 for 24 h. The mRNA expression of pS2, which is the one gene whose expression is upregulated by E2, was analyzed using the quantitative polymerase chain reaction (Supporting Information). The relative pS2 mRNA expression levels of the cells treated with each peptide are summarized in Figure 3. The R7-unconjugated (nonmembrane-penetrating) peptides **1**–**3** and the heptaarginine (YR7)[27] peptide did not inhibit transcription. On the other hand, the mRNA expression of pS2 was significantly decreased (by 87%) by the addition of 3 μM of the R7-conjugated peptide **5**. Treatment with 3 μM of the R7-conjugated peptide **4** did not suppress the mRNA expression of pS2 at all, but treatment with 10 μM of **4** decreased it by 95% (Supporting Information). Conversely, treatment with the R7-conjugated peptide **6** at concentrations ranging from 3 μM to 10 μM did not induce any significant reduction in ER-mediated transcriptional activity. These results demonstrated that the R7-conjugated peptides **4** and **5** were able to exhibit antagonistic effects on ER-mediated transcription at the cellular level, and **5** displayed particularly potent inhibitory activity.

The inhibitory activity of peptides **4** and **5** against ER–coactivator interactions were evaluated using EnBio receptor cofactor assay systems (RCAS) for ERα (Fujikura Kasei Co., Ltd.) according to the manufacturer's instructions (Figure 4). The R7-unconjugated peptides **1** and **2** demonstrated strong activity against ERα–coactivator interactions. While the activities of the corresponding R7-conjugated peptides **4** and **5** were reduced, peptide **5** still demonstrated strong activity (IC_{50}: 94 nM). These results indicated that peptides **4** and **5** suppress ER-mediated transcription by inhibiting ERα–coactivator interactions. The R7-conjugated peptide **5** exhibited stronger inhibitory activity against ERα–coactivator interactions than **4**, and therefore, **5** was able to suppress ER-mediated transcription more efficiently than **4**, even at the cellular level.

The dominant conformations of peptides **1**–**6** were analyzed by assessing their CD spectra in 20% aqueous 2,2,2-trifluoroethanol (TFE) solution (Figure 5). The CD spectra of peptides **1** and **2**, and those of their R7-conjugated peptides **4** and **5**, displayed negative maxima at around 208 and 222 nm, indicating that all of the peptides formed stable right-handed α-helical structures. These findings suggested that the R7 fragment did not disrupt helix formation. On the other hand, the SRC-1 peptide **3** and its R7-conjugated form **6** were found to be composed of random coil structures rather than α-helices. These results indicated that peptides require stabilized helical structures in order to possess significant inhibitory activity against ER-coactivator interactions.

CONCLUSION

In conclusion, we developed heptaarginine (R7)-conjugated PERM as molecules that could be used to suppress ER-mediated transcription at the cellular level. The R7-conjugated peptides were able to enter ER-positive T47D cells efficiently, and one of them, peptide **5**, downregulated the mRNA expression of pS2 by 87% at a dose of 3 μM. Furthermore, **5** displayed strong inhibitory activity (IC_{50}: 94 nM) against ER–coactivator interactions. Although the inhibitory activity of the R7-conjugated peptide **5** against ER–coactivator interactions was slightly decreased compared with that of the R7-unconjugated peptide **2** (IC_{50}: 13 nM), **5** still exhibited potent activity. The dominant conformations of the peptides were analyzed based on

Table 1. Sequences of Peptides 1–7

peptide	sequence
PERM-1 (**1**)	H-Lys-*cyclo*(D-Cys-Ile-Leu-Cys)-Arg-Leu-Leu-Gln-NH_2
PERM-3 (**2**)	H-Arg-*cyclo*(D-Cys-Ile-Leu-Cys)-Arg-Npg[a]-Leu-Gln-NH_2
SRC-1[b] (**3**)	H-His-Lys-Ile-Leu-His-Arg-Leu-Leu-Gln-NH_2
PERM-1-R7 (**4**)	H-Lys-*cyclo*(D-Cys-Ile-Leu-Cys)-Arg-Leu-Leu-Gln-$(Gly)_3$-$(Arg)_7$-NH_2
PERM-3-R7 (**5**)	H-Arg-*cyclo*(D-Cys-Ile-Leu-Cys)-Arg-Npg-Leu-Gln-$(Gly)_3$-$(Arg)_7$-NH_2
SRC-1-R7 (**6**)	H-His-Lys-Ile-Leu-His-Arg-Leu-Leu-Gln-$(Gly)_3$-$(Arg)_7$-NH_2
YR7 (**7**)	H-Tyr-$(Arg)_7$-NH_2

[a]Npg: neopentylglycine. [b]The LXXLL motif of the coactivator.

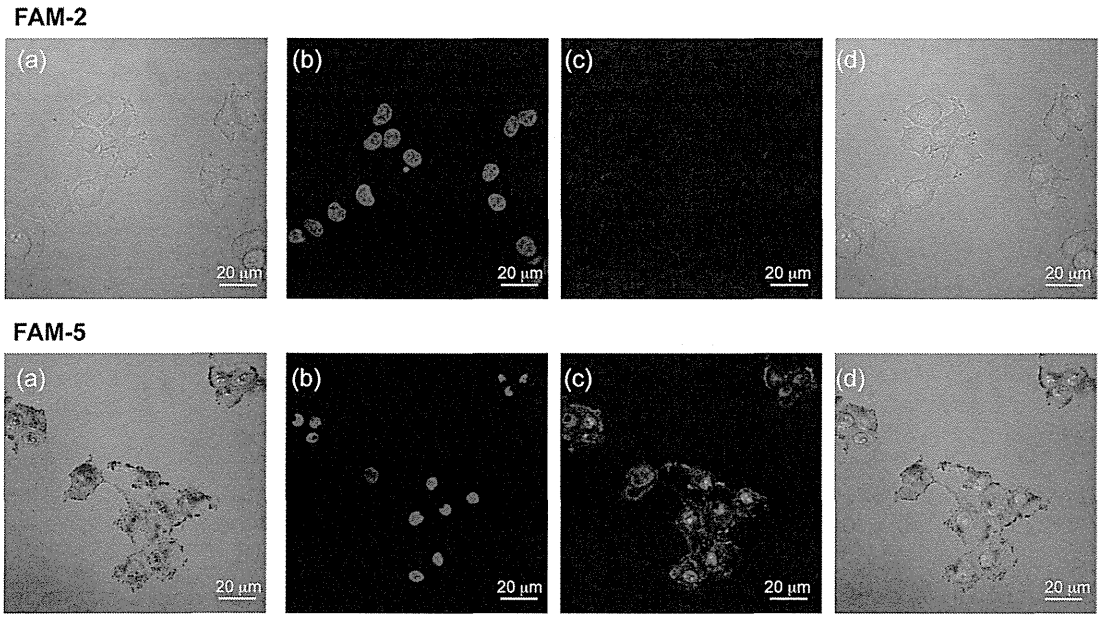

Figure 2. CLSM images of T47D cells that had been treated with **FAM-2** or **FAM-5** (peptide concentration: 1 μM, incubation time: 3 h). (a) Bright-field images, (b) nuclei stained with Hoechst 33342 (blue), (c) the intracellular distribution of the FAM-conjugated peptides (green), and (d) merged images.

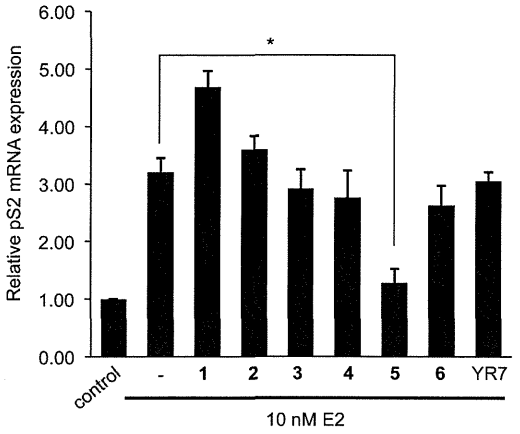

Figure 3. Inhibition of ERα-mediated gene expression in T47D cells. Peptide concentration: 3 μM. The error bars represent standard deviation, $n = 3$. $^*p < 0.05$.

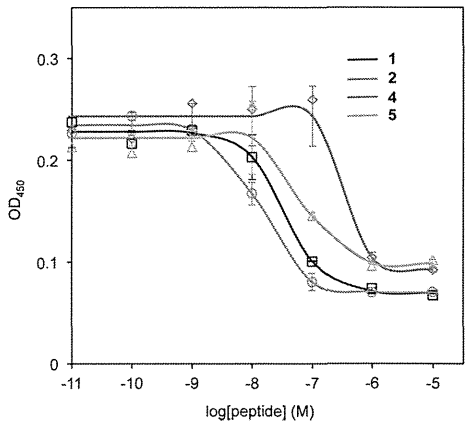

Peptide	IC_{50} (nM)
1	35
2	13
4	749
5	94

The EC_{50} value of the positive control, E2, was 1.5 nM.

Figure 4. IC_{50} values of peptides against ERα–cofactor interactions according to RCAS.

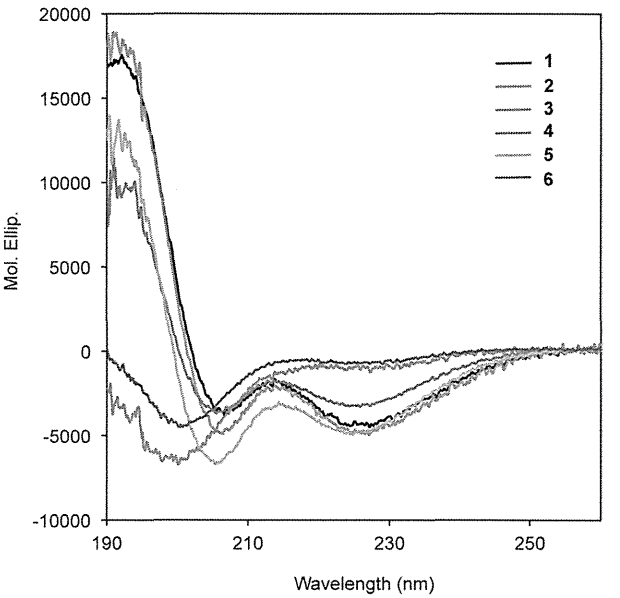

Figure 5. CD spectra of peptides **1**–**6** in the 190–260 nm region. Peptide concentration: 100 μM in 20% aqueous TFE solution.

their CD spectra, and it was found that **5** formed a right-handed α-helical structure similar to that of the R7-unconjugated peptide **2**. The R7-conjugation of the PERM did not disrupt their helical structures. These results indicate that the conjugation of PERM to R7 would aid the development of novel inhibitors of ER-mediated transcription at the cellular level. The derivatization of further helical peptides and detailed studies of their inhibitory mechanisms are currently underway.

■ ASSOCIATED CONTENT

Supporting Information

Information about the synthesis and purification of the peptides and the protocols of the in vitro assays. This material is available free of charge via the Internet at http://pubs.acs.org.

dx.doi.org/10.1021/bc500480e | *Bioconjugate Chem.* 2014, 25, 1921–1924